Since January 2020 Elsevier has created a COVID-19 resource centre with free information in English and Mandarin on the novel coronavirus COVID-19. The COVID-19 resource centre is hosted on Elsevier Connect, the company's public news and information website.

Results in Control and Optimization 7 (2022) 100115

Contents lists available at ScienceDirect

Results in Control and Optimization

journal homepage: www.elsevier.com/locate/rico

Optimal control design incorporating vaccination and treatment on six compartment pandemic dynamical system

R. Prem Kumar [a,b], Sanjoy Basu [c], P.K. Santra [d], D. Ghosh [a], G.S. Mahapatra [a,*]

[a] Department of Mathematics, National Institute of Technology Puducherry, Karaikal 609609, India
[b] Department of Mathematics, Avvaiyar Government College for Women, Karaikal 609602, Puducherry, India
[c] Department of Mathematics, Arignar Anna Government Arts and Science College, Karaikal 609605, Puducherry, India
[d] Maulana Abul Kalam Azad University of Technology, Kolkata 700064, India

ARTICLE INFO

MSC:
92B05

Keywords:
Equilibrium points
Basic reproduction number
Local and global stability
Optimal control
Novel coronavirus

ABSTRACT

In this paper, a mathematical model of the COVID-19 pandemic with lockdown that provides a more accurate representation of the infection rate has been analyzed. In this model, the total population is divided into six compartments: the susceptible class, lockdown class, exposed class, asymptomatic infected class, symptomatic infected class, and recovered class. The basic reproduction number (R_0) is calculated using the next-generation matrix method and presented graphically based on different progression rates and effective contact rates of infective individuals. The COVID-19 epidemic model exhibits the disease-free equilibrium and endemic equilibrium. The local and global stability analysis has been done at the disease-free and endemic equilibrium based on R_0. The stability analysis of the model shows that the disease-free equilibrium is both locally and globally stable when $R_0 < 1$, and the endemic equilibrium is locally and globally stable when $R_0 > 1$ under some conditions. A control strategy including vaccination and treatment has been studied on this pandemic model with an objective functional to minimize. Finally, numerical simulation of the COVID-19 outbreak in India is carried out using MATLAB, highlighting the usefulness of the COVID-19 pandemic model and its mathematical analysis.

1. Introduction

1.1. General statement

A new infectious disease known as coronavirus disease (COVID-19) was reported first time on 30 January 2020 in India as an outbreak of severe acute respiratory syndrome (SARS) [1]. The virus that causes this transmittable disease is mainly transmitted through dewdrops generated when an infected person coughs, sneezes, or exhales. There is a chance of infection of COVID-19 by breathing in the virus if you are adjacent to someone who has COVID-19 infection or by touching a contaminated surface and then your mouth, eyes, or nose. That is why it is essential to wear a mask in the mouth and sanitize the hands rigorously of every person to rescue them from this infection. Most infected people pass through some mild to moderate symptoms of coronavirus and recover without special treatment. There are two types of the infected population; one is an exposed infected population with some mild to moderate symptoms of coronavirus, and another is an asymptotically infected population with no symptoms so that directly we cannot recognize them. Since this is the 21st century's largest outbreak globally, most countries are perceiving a surge in their daily COVID-19 disease tally. To avoid the continuous spread of the disease and break the chain, several lockdowns, announcing

* Correspondence to: Department of Mathematics, National Institute of Technology Puducherry, Karaikal 609609, Puducherry, India.
E-mail address: gs.mahapatra@nitpy.ac.in (G.S. Mahapatra).

https://doi.org/10.1016/j.rico.2022.100115
Received 20 September 2021; Received in revised form 21 January 2022; Accepted 23 March 2022
Available online 31 March 2022

several guidelines, aggressive testing, vaccination, and timely provision of medicines are some ways governments are trying to impose on the population. The current Scenario and impact of COVID-19 in India have been discussed by Kumar et al. [2], Jachak et al. [3], Pradhan et al. [4], Asad et al. [5] and Sarkar et al. [6]. Impact of COVID-19 outbreak on extreme hot climate in India has been studied by Sasikumar et al. [7]; and Bhadra et al. [8] investigated the effect of population density on COVID-19 infected and mortality rate in India. According to MOHFW [9], Govt. of India, the first COVID-19 vaccine was launched on 16th January 2021 in India. The Serum Institute of India has locally manufactured the Oxford-Astra Zeneca vaccine to fight against COVID-19 in India. At the same time, Bharat Biotech, the vaccine's manufacturer, has produced India's Covaxin for the same purpose. After launching the COVID-19 vaccine in India, healthcare and front-line workers are given the first preference, and then the persons over 60 years of age. Besides that, planning with the modern mathematical epidemiological model and the preventive control analysis is very important to break the chain of the continuous spread of the disease. We have to study the mechanism of this viral disease transmission and how to control the spread of the virus.

1.2. Different epidemiology models

Global analysis of an epidemiological model with varying populations and vaccination has been studied by Yang et al. [10] and Sun et al. [11]. Zhou and Cui [12] investigated the stability and bifurcation analysis for an epidemic SEIR model with a saturated recovery rate. The persistence of the HIV disease model has been discussed by Busenberg et al. [13] and Samanta [14]. Cai et al. [15] analyzed the extended HIV disease model with treatment. The stability analysis of cholera epidemic models has been discussed by Tian and Wang [16]. Bai and Zhou [17] analyzed an epidemic SEIRS model with vaccination and seasonally contact rate. Lahrouz et al. [18] explained the global stability for a SIRS epidemic model with vaccination. An SEIR epidemic system including media impact with relapse and nonlinear incidence rate has been explained by Wang et al. [19], and also by Khyar and Allali [20]. Then a simple mathematical model for fitting mild, severe, and known cases during the current COVID-19 epidemic has been considered by Betti and Heffernan [21]. Nadim et al. [22] analyzed a compartmental epidemic model of COVID-19 to predict and control the outbreak. Tian et al. [23] investigated the spread and control of COVID-19 using a data set. Li et al. [24] developed and analyzed a SEIQR difference-equation COVID-19 epidemic mode1. Sun et al. [25] explored the effects of lockdown and medical resources on the COVID-19 transmission in Wuhan. The transmissibility of the COVID-19 mathematical model has been studied by Chen et al. [26], Mumbu et al. [27], Rezapour et al. [28] and Wijaya et al. [29]. A critical analysis of the SIR epidemic model has been explained by Comunian et al. [30]. Engbert et al. [31] and Rihan et al. [32] studied the stochastic epidemic mathematical model for novel coronavirus infection. Carvalho and Pinto [33] studied the importance of quarantine in COVID-19 pandemic. The dynamical transmission of the coronavirus model has been analyzed by Memarbashi and Mahmoundi [34] and Farman et al. [35]. A state-space method is used by Koyama et al. [36] to find the time-varying reproduction number of COVID-19. A case study COVID-19 epidemic in Egypt using machine learning has been discussed by Amar et al. [37] and another case study with a mathematical model for the same pandemic in India has been explained by Biswas et al. [38]. Then network-based COVID-19 disease spreading in Italy has been discussed by Pizzuti et al. [39]. The only effect of lockdown in the COVID-19 pandemic has been studied by many scientists [40–42]. De Sousa et al. [43] discussed the Kinetic Monte Carlo COVID-19 epidemic model with the impact of mobility restriction. A SEIAR COVID-19 epidemic model with confinement and quarantine has been proposed by De la Sen et al. [44] and Yuan et al. [45]. Hikal et al. [46] analyzed the stability of the COVID-19 epidemic model with fractional-order derivatives whereas the delay in implementing the quarantine policy. Mishra et al. [47] studied the three novel quarantine epidemic systems for the spread of novel coronavirus worldwide. A SIHR epidemic model with population size dependent contact rate has been analyzed by Jiao and Huang [48]. During the same pandemic, the bed allocation strategy in hospital-based on queuing theory has been studied by Hu et al. [49]. Modeling of control strategy depending on test, trace and quarantine for the coronavirus disease in a state of Brazil has been discussed by Amaku et al. [50]. Then different control strategies for the COVID-19 epidemic have been optimized by many mathematician [51–62]. The impact of influenza vaccination in public health for the COVID-19 epidemic has been analyzed by Li et al. [63]. Gonçalves et al. [64] considered the dynamical analysis on COVID-19 disease in non-human primates.

1.3. Uniqueness of proposed COVID-19 model

Our study analyzed the stability analysis of the new COVID-19 epidemic model with lockdown effect and the same natural death rate in each class that provides a more accurate representation of the infection rate. The basic reproduction number is calculated based on some parameter table values with different progression rates and effective contact rates of infective individuals; and presented graphically. After lockdown, we discussed this mathematical epidemiological model with three controls: vaccination control on exposed class, treatment control on asymptomatic infected class, and another treatment control on symptomatic infected class. First, optimal control represents the vaccination been applied on exposed population, second optimal control represents the recovery rate of the symptomatic infected individuals under treatment, and third optimal control represents the recovery rate of the asymptomatic infected individuals under treatment. Then, the objective function is defined for the three optimal control systems to minimize the effect of infection on exposed, asymptotic, and symptomatic infected phases.

2. Formulation of six-compartmental pandemic model

In this section, a six-compartmental model has been studied. To derive a realistic model, we divide the total population $N(t)$ in to six different classes, namely, susceptible class $S(t)$, lockdown class $L(t)$, exposed class $E(t)$, infected but asymptomatic class $I_A(t)$,

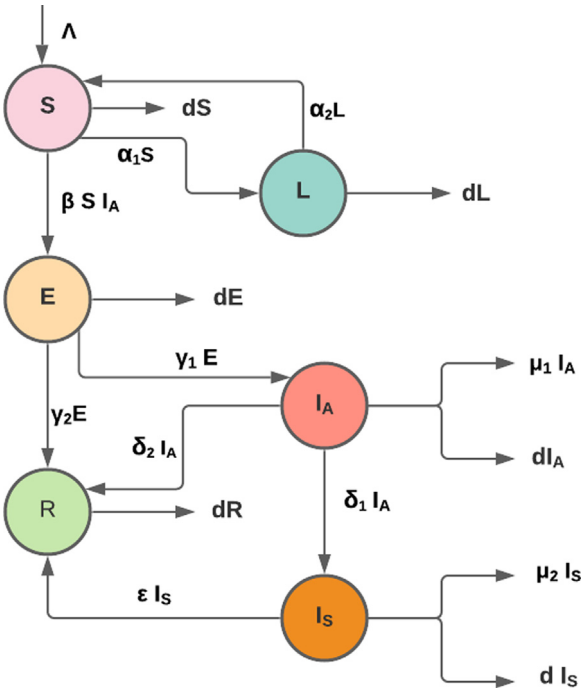

Fig. 1. Flow diagram of the mathematical pandemic model.

Table 1
Parameters of the COVID-19 pandemic mathematical model with meaning.

Parameter	Description
Λ	Recruitment rate of new individuals
α_1	The progression rate from the susceptible class to the lockdown class
α_2	The progression rate from the lockdown class to the susceptible class
β	Effective contact rate of asymptomatic infective individuals
d	Natural death rate in each class
γ_1	Rate of exposed individuals gets infected and remain asymptotic to COVID-19
γ_2	Rate of exposed individuals get recovered
δ_1	Rate of asymptotic infected individuals become symptomatic to the disease
δ_2	Rate of asymptomatic infected individuals gets recovered
μ_1	Death rate of the asymptomatic infected individuals due to the COVID-19 disease
μ_2	Death rate of symptomatic infected individuals due to the COVID-19 disease
ϵ	Recovery rate of the symptomatic infected individuals

infected but symptomatic class $I_S(t)$ and recovered class $R(t)$. The transfer diagram of the proposed pandemic model is represented in Fig. 1.

The COVID-19 pandemic model has the following assumptions (see Table 1):

(a) The susceptible population (S) consists of humans who are not yet infected by COVID-19 disease. Still, it is assumed that the humans of this class are infected when there is an effective contact with asymptomatic infected individuals (I_A) and the transmission rate of infection is given by $\beta S I_A$.

(b) The lockdown population (L) consists of humans moving from susceptible class and confine due to lockdown, and the rate of transmission from susceptible class is given by $\alpha_1 S$ and move out from the lockdown class (L) to the susceptible class with the transmission rate $\alpha_2 L$.

(c) The exposed population (E) is composed of humans who are infected by COVID-19 disease and are not capable of spreading the disease. After testing positive for COVID-19 disease, the humans are assumed to be asymptomatic and move to the asymptomatic infected class (I_A) with the rate of transmission given by $\gamma_1 E$. Some humans of this class naturally recover from COVID-19 disease and move to the recovered class (R) with the transmission rate $\gamma_2 E$.

(d) The asymptomatic infected individuals (I_A) is composed of humans who are infected with COVID-19 disease without any symptoms. The humans of this class, after symptoms, appear move to the symptomatic infected class (I_S) with the rate of transmission $\delta_1 I_A$. Some humans of this class naturally recover from the disease and move to the recovered class (R) with the transmission rate $\delta_2 I_A$.

(e) The symptomatic infected individuals (I_S) is composed of humans who are infected with COVID-19 disease with symptoms of the disease. Some humans of this class recover from COVID-19 disease who are under treatment and move to the recovered class (R) with the rate of transmission given by ϵI_S.

(f) It is assumed that in every compartment, the natural death of humans occurs. In the compartments, I_A and I_S there exists the death of humans related to the COVID-19 disease in addition to the natural death.

A mathematical model of COVID-19 that provides a more accurate representation of the infection rate, which is useful for prevention and control, is given by the following system of nonlinear differential equations:

$$\begin{cases} \frac{dS}{dt} &= \Lambda + \alpha_2 L - \left(\alpha_1 + d\right) S - \beta S I_A \\ \frac{dL}{dt} &= \alpha_1 S - \left(\alpha_2 + d\right) L \\ \frac{dE}{dt} &= \beta S I_A - \left(\gamma_1 + \gamma_2 + d\right) E \\ \frac{dI_A}{dt} &= \gamma_1 E - \left(\delta_1 + \delta_2 + \mu_1 + d\right) I_A \\ \frac{dI_S}{dt} &= \delta_1 I_A - \left(d + \mu_2 + \epsilon\right) I_S \\ \frac{dR}{dt} &= \gamma_2 E + \delta_2 I_A + \epsilon I_S - dR \end{cases} \tag{1}$$

Here all coefficients are positive with their initial conditions :

$$S(0) > 0; L(0) > 0; E(0) \geq 0; I_A(0) \geq 0; I_S(0) \geq 0; R(0) \geq 0 \tag{2}$$

3. Basic properties of the model

3.1. Non-negativity solutions

Theorem 1. *All solution of the system (1) with initial conditions (2) are non-negative for all $t \geq 0$.*

Proof. The functions on the right-hand side of the system (1) are completely continuous and locally Lipschitzian on C^1, and hence the unique solution $(S(t), L(t), E(t), I_A(t), I_S(t), R(t))$ of the system (1) with the initial conditions (2) exists on the interval $[0, u)$ where $0 < u \leq \infty$. From the first equation of the system (1) with $S(0) > 0$, we get $\frac{dS}{dt} > -\left(\alpha_1 + d + \beta I_A\right) S$ and hence $S(t) > S(0)e^{-\int_0^t \psi(I_A(x))dx} > 0$, where $\psi(I_A) = \alpha_1 + d + \beta I_A(x)$. Integrating the second equation of (1) with $L(0) > 0$, we get $\frac{dL}{dt} > -(\alpha_2 + d)L$, and hence $L(t) > L(0)e^{-(\alpha_2+d)t} > 0$. From the remaining equations of the system (1) with $E(0) \geq 0$, $I_A(0) \geq 0$, $I_S(0) \geq 0$ and $R(0) \geq 0$, we get $\frac{dE}{dt} \geq -(\gamma_1 + \gamma_2 + d)E$, $\frac{dI_A}{dt} \geq -(\delta_1 + \delta_2 + \mu_1 + d)I_A$, $\frac{dI_S}{dt} \geq -(d + \mu_2 + \epsilon)I_S$, $\frac{dR}{dt} \geq -dR$ and hence after integrating, we get $E(t) \geq E(0)e^{-(\gamma_1+\gamma_2+d)t} \geq 0$, $I_A(t) \geq I_A(0)e^{-(\delta_1+\delta_2+\mu_1+d)t} \geq 0$, $I_S(t) \geq I_S(0)e^{-(d+\mu_2+\epsilon)t} \geq 0$ and $R(t) \geq R(0)e^{-dt} \geq 0$. Hence the proof. □

3.2. Invariant region of the system and boundedness

Theorem 2. *All solutions of the system (1) which lies in $\mathbb{R}^6_+$ are uniformly bounded and are restricted to the invariant region $D = \{(S, L, E, I_A, I_S, R) \in \mathbb{R}^6_+ : 0 < Q(t) \leq \frac{\Lambda}{h}\}$ as $t \to \infty$, where $h \leq d$ and $Q(t) = S(t) + L(t) + E(t) + I_A(t) + I_S(t) + R(t)$.*

Proof. Let us assume that (S, L, E, I_A, I_S, R) be the solution of (1). Let $Q(t) = S(t) + L(t) + E(t) + I_A(t) + I_S(t) + R(t)$. The time derivative of $Q(t)$ is given by $\frac{dQ}{dt} = \Lambda - dQ - \mu_1 I_A - \mu_2 I_S$. Hence for each $h > 0$, we have $\frac{dQ}{dt} + hQ = \Lambda - (d - h)Q - \mu_1 I_A - \mu_2 I_S$. For $h \leq d$, we get $\frac{dQ}{dt} + hQ \leq \Lambda$. Applying the theory of differential inequality [65], we get $0 < Q(S, L, E, I_A, I_S, R) \leq \frac{\Lambda}{h}(1 - e^{-ht}) + Q(S(0), L(0), E(0), I_A(0), I_S(0), R(0))e^{-ht}$ which yields, $0 < Q \leq \frac{\Lambda}{h}$ as $t \to \infty$. Thus every solution of (1) which pledge in $\mathbb{R}^6_+$ are uniformly bounded and restricted to the region $D = \{(S, L, E, I_A, I_S, R) \in \mathbb{R}^6_+ : 0 < Q(t) \leq \frac{\Lambda}{h}\}$. Hence the region D with the initial conditions (2) is a positively invariant region under the flow induced by the system (1) in $\mathbb{R}^6_+$. □

Remark 3. Since every solution of (1) have non-negative components with non-negative initial values in D for t ≥ 0 and globally attracting in $\mathbb{R}^6_+$ based on the system (1), and further, the last equation of the system (1) does not depend on the other equations, we confine our attention to the dynamics of the system (1) without involving the last compartment in $\Gamma = \{(S, L, E, I_A, I_S) \in \mathbb{R}^5_+ : 0 < S(t) + L(t) + E(t) + I_A(t) + I_S(t) \leq \frac{\Lambda}{h}\}$. Thus the system (1) defined on Γ is well-posed mathematically and epidemiologically. So, it is sufficient to study the dynamics of the system (1) defined on Γ.

4. Equilibrium points of the system and its existence

To find the equilibria of the system (1), we set the right hand side of the system to equal zero. Then we get two equilibria in the coordinate (S, L, E, I_A, I_S): (i) Disease-free equilibrium (DFE) $P_0(S_0, L_0, 0, 0, 0)$ where, $S_0 = \frac{\Lambda(\alpha_2+d)}{d(\alpha_1+\alpha_2+d)}$ and $L_0 = \frac{\Lambda\alpha_1}{d(\alpha_1+\alpha_2+d)}$. It is

observed that DFE P_0 always exists. (ii) The endemic equilibrium (EE) $P_1(S^*, L^*, E^*, I_A^*, I_S^*)$ with positive components: $S^* = \frac{c_1c_2}{\beta\gamma_1}$, $L^* = \frac{\alpha_1c_1c_2}{c_4\beta\gamma_1}$, $E^* = \frac{\gamma_1\Lambda\beta c_4 - dc_3c_1c_2}{\beta\gamma_1c_4c_1}$, $I_A^* = \frac{\Lambda\gamma_1\beta c_4 - dc_1c_2c_3}{c_1c_2c_4\beta}$, $I_S^* = \frac{\delta_1(\gamma_1\Lambda\beta c_4 - dc_3c_1c_2)}{c_1c_2c_4c_5\beta}$, where $c_1 = d + \gamma_1 + \gamma_2$, $c_2 = d + \delta_1 + \delta_2 + \mu_1$, $c_3 = d + \alpha_1 + \alpha_2$, $c_4 = d + \alpha_2$, $c_5 = d + \epsilon + \mu_2$, $c_6 = \alpha_1 + d_1$. Clearly $S^* > 0$, $L^* > 0$ but E^*, I_A^* and I_S^* are positive if $\gamma_1\Lambda\beta c_4 - dc_3c_1c_2 > 0$. If we set $R_0 = \frac{\gamma_1\beta\Lambda c_4}{d(c_1c_2c_3)}$, then $\gamma_1\Lambda\beta c_4 - dc_3c_1c_2 > 0$ if $R_0 > 1$ and hence $E^* = \frac{dc_2c_3(R_0-1)}{\beta\gamma_1c_4}$, $I_A^* = \frac{dc_3(R_0-1)}{\beta c_4}$ and $I_S^* = \frac{\delta_1dc_3(R_0-1)}{c_4c_5\beta}$ which are positive . Hence the EE point P_1 exists if $R_0 > 1$.

5. Basic reproduction number R_0

This section represents the basic reproduction number, denoted by R_0, that is "the number of secondary cases which one case would produce in a completely susceptible population" [66]. Using the method of next generation matrix [67], we determine the expression for R_0 at $P_0(S_0, L_0, 0, 0, 0)$. Let $x = (E, I_A, I_S, S, L)^T$, then the system (1) can be written as

$$\frac{dx}{dt} = \mathcal{F}(x) - \mathcal{V}(x)$$

where $\mathcal{F}(x) = \begin{pmatrix} \beta S I_A \\ 0 \\ 0 \\ 0 \\ 0 \end{pmatrix}$, and $\mathcal{V}(x) = \begin{pmatrix} c_1E \\ -\gamma_1E + c_2I_A \\ -\delta_1I_A + c_5I_S \\ -\Lambda - \alpha_2L + (\alpha_1 + \beta I_A + d)S \\ -\alpha_1S + c_4L \end{pmatrix}$.

The Jacobian matrices of $\mathcal{F}(x)$ and $\mathcal{V}(x)$ at the DFE P_0 are given by

$$D\mathcal{F}(P_0) = \begin{pmatrix} 0 & \frac{\beta\Lambda c_4}{dc_3} & 0 & 0 & 0 \\ 0 & 0 & 0 & 0 & 0 \\ 0 & 0 & 0 & 0 & 0 \\ 0 & 0 & 0 & 0 & 0 \\ 0 & 0 & 0 & 0 & 0 \end{pmatrix}, \text{ and } D\mathcal{V}(P_0) = \begin{pmatrix} c_1 & 0 & 0 & 0 & 0 \\ -\gamma_1 & c_2 & 0 & 0 & 0 \\ 0 & -\delta_1 & c_5 & 0 & 0 \\ 0 & \frac{\beta\Lambda c_4}{dc_3} & 0 & c_6 & -\alpha_2 \\ 0 & 0 & 0 & -\alpha_1 & c_4 \end{pmatrix}.$$

Then the matrices F and V can be written as

$$F = \begin{pmatrix} 0 & \frac{\beta\Lambda c_4}{dc_3} & 0 \\ 0 & 0 & 0 \\ 0 & 0 & 0 \end{pmatrix}, \; V = \begin{pmatrix} c_1 & 0 & 0 \\ -\gamma_1 & c_2 & 0 \\ 0 & -\delta_1 & c_5 \end{pmatrix}, \text{ and } FV^{-1} = \begin{pmatrix} \frac{\beta\Lambda c_4\gamma_1}{dc_1c_2c_3} & \frac{\beta\Lambda c_4}{dc_2c_3} & 0 \\ 0 & 0 & 0 \\ 0 & 0 & 0 \end{pmatrix}.$$

The spectral radius of FV^{-1} is $\rho(FV^{-1})$ which is the basic reproduction number $R_0 = \rho(FV^{-1}) = \frac{\beta\Lambda c_4\gamma_1}{dc_1c_2c_3}$.

6. Local stability analysis

6.1. Local stability of DFE

Theorem 4. *The DFE P_0 of (1) is locally asymptotically stable if $R_0 < 1$ and unstable if $R_0 > 1$.*

Proof. The Jacobian matrix of (1) at P_0 is given by

$$J(P_0) = \begin{pmatrix} -c_6 & \alpha_2 & 0 & -\frac{\beta\Lambda c_4}{dc_3} & 0 \\ \alpha_1 & -c_4 & 0 & 0 & 0 \\ 0 & 0 & -c_1 & \frac{\beta\Lambda c_4}{dc_3} & 0 \\ 0 & 0 & \gamma_1 & -c_2 & 0 \\ 0 & 0 & 0 & \delta_1 & -c_5 \end{pmatrix}$$

Eigenvalues of the above matrix are $\lambda_1 = -c_5 < 0$, $\lambda_2 = -c_3 < 0$, $\lambda_3 = -d < 0$, $\lambda_4 = -\frac{c_1+c_2+\sqrt{(c_1-c_2)^2+\frac{4c_4\beta\gamma_1\Lambda}{dc_3}}}{2} < 0$ and $\lambda_5 = \frac{-(c_1+c_2)+\sqrt{(c_1-c_2)^2+\frac{4c_4\beta\gamma_1\Lambda}{dc_3}}}{2}$. But $\lambda_5 < 0$ if and only if $\frac{4c_4\beta\gamma_1\Lambda}{dc_3} < 4c_1c_2$. But $\frac{4c_4\beta\gamma_1\Lambda}{dc_3} < 4c_1c_2$ if and only if $R_0 < 1$. Hence P_0 is stable if $R_0 < 1$ and unstable if $R_0 > 1$. □

6.2. Local stability of EE

The local stability of the endemic equilibrium P_1 is proved using the Routh–Hurwitz criterion [68,69].

Theorem 5. *If $R_0 > 1$, then the EE P_1 of (1) exists and is locally asymptotically stable if it satisfies the condition $A_1A_2A_3 - A_3^2 - A_1^2A_4 > 0$, where $c_1 = d + \gamma_1 + \gamma_2$, $c_2 = d + \delta_1 + \delta_2 + \mu_1$, $c_3 = d + \alpha_1 + \alpha_2$, $c_4 = d + \alpha_2$, $c_5 = d + \epsilon + \mu_2$, $c_6 = \alpha_1 + d_1$, $k_1 = \alpha_1 + \beta I_A^* + d$, $k_2 = \beta S^*$, $k_3 = \beta I_A^*$, $A_1 = c_1 + c_2 + c_4 + k_1$, $A_2 = (c_4k_1 - \alpha_1\alpha_2) + (c_1 + c_2)(c_4 + k_1)$, $A_3 = (c_1 + c_2)(c_4k_1 - \alpha_1\alpha_2) + k_2k_3\gamma_1$, $A_4 = c_4(c_1c_2k_1 + c_6k_2\gamma_1)$.*

Proof. The Jacobian matrix of (1) at P_1 is given by

$$J(P_1) = \begin{pmatrix} -k_1 & \alpha_2 & 0 & -k_2 & 0 \\ \alpha_1 & -c_4 & 0 & 0 & 0 \\ k_3 & 0 & -c_1 & k_2 & 0 \\ 0 & 0 & \gamma_1 & -c_2 & 0 \\ 0 & 0 & 0 & \delta_1 & -c_5 \end{pmatrix}$$

The characteristic equation of the above jacobian matrix is given by $(\lambda+c_5)(\lambda^4+A_1\lambda^3+A_2\lambda^2+A_3\lambda+A_4)=0$, where $k_1=\alpha_1+\beta I_A^*+d$, $k_2=\beta S^*$, $k_3=\beta I_A^*$, $A_1=c_1+c_2+c_4+k_1>0$, $A_2=(c_4k_1-\alpha_1\alpha_2)+(c_1+c_2)(c_4+k_1)$, $A_3=(c_1+c_2)(c_4k_1-\alpha_1\alpha_2)+k_2k_3\gamma_1$, $A_4=k_2k_3c_4\gamma_1>0$. Clearly one of the roots of the characteristic equation of $J(P_1)$ is -$c_5<0$. The remaining roots can be determined from the following equation $\lambda^4+A_1\lambda^3+A_2\lambda^2+A_3\lambda+A_4=0$. Analyzing the polynomial by using the Routh–Hurwitz criterion [69], we get that the EE P_1 is locally asymptotically stable if $A_i>0$ for $i=1,3,4$ and $A_1A_2A_3-A_3^2-A_1^2A_4>0$. Since $c_4k_1-\alpha_1\alpha_2>0$ and $c_1c_2-k_2\gamma_1=0$, we get $A_i>0$ for $i=1,2,3,4$. The equilibrium point P_1 exists iff $R_0>1$ and is locally asymptotically stable if it satisfies the condition $A_1A_2A_3-A_3^2-A_1^2A_4>0$. □

7. Global stability analysis of the model

7.1. Global stability of DFE

Theorem 6. *The DFE P_0 of the system (1) is globally asymptotically stable if $R_0<1$.*

Proof. Since P_0 is locally asymptotically stable when $R_0<1$, it is sufficient to show that P_0 is globally attractive. In Section 3, it has been proved that every solution of (1) is non-negative and bounded. For a bounded and continuous real valued function $g(t)$ (say) defined on $\mathbb{R}^+$, let $\overline{g}=\limsup_{t\to\infty} g(t)$ and $\underline{g}=\liminf_{t\to\infty} g(t)$. Hence by the Fluctuation lemma [70] (using the following notations in [70]), there is a sequence $\sigma_n\to\infty$ such that $S(\sigma_n)\to\overline{S}$ and $S'(\sigma_n)\to 0$ whenever $n\to\infty$. From the first equation of (1), we get

$$S'(\sigma_n)+c_6S(\sigma_n)+\beta S(\sigma_n)I_A(\sigma_n)=\Lambda+\alpha_2L(\sigma_n). \tag{3}$$

Letting $n\to\infty$, we get

$$c_6\overline{S}\le(c_6+\beta\overline{I_A})\overline{S}\le\Lambda+\alpha_2\overline{L} \tag{4}$$

and using the remaining equations of (1), we get the following

$$c_4\overline{L}\le\alpha_1\overline{S} \tag{5}$$

$$c_1\overline{E}\le\beta\overline{S}\,\overline{I_A} \tag{6}$$

$$c_2\overline{I_A}\le\gamma_1\overline{E} \tag{7}$$

$$c_5\overline{I_S}\le\delta_1\overline{I_A} \tag{8}$$

$$d\overline{R}\le\gamma_2\overline{E}+\epsilon\overline{I_S}+\delta_2\overline{I_A} \tag{9}$$

Next, we shall show that $\overline{E}=0$. Suppose that $\overline{E}>0$, using (6) and (7), we get $c_1\overline{E}\le\beta\overline{S}\,\overline{I_A}\le\frac{\gamma_1\beta}{c_2}\overline{S}\,\overline{E}$. Since $\overline{E}>0$, we get $\overline{S}\ge\frac{c_1c_2}{\beta\gamma_1}=\frac{\Lambda c_4}{dc_3}.\frac{1}{R_0}$. Since $R_0<1$, we get $\overline{S}>\frac{\Lambda c_4}{dc_3}$. From (3) and (4), we get $c_6\overline{S}\le\Lambda+\alpha_2\overline{L}\le\Lambda+\frac{\alpha_1\alpha_2}{c_4}\overline{S}$ and hence $\overline{S}\le\frac{\Lambda c_4}{dc_3}$. Therefore, $\frac{\Lambda c_4}{dc_3}<\overline{S}\le\frac{\Lambda c_4}{dc_3}<\frac{\Lambda}{d}$, a contradiction. Hence $\overline{E}=0$ and hence $\lim_{t\to0}E(t)=0$. Suppose $\overline{I_A}>0$, then using (6) and (7), we get $\beta\overline{S}\,\overline{I_A}\ge c_1\overline{E}\ge\frac{c_2c_1}{\gamma_1}\overline{I_A}$. Since $\overline{I_A}>0$, we get $\overline{S}\ge\frac{c_1c_2}{\beta\gamma_1}=\frac{dc_1c_2c_3}{\beta\gamma_1\Lambda c_4}\left(\frac{\Lambda c_4}{dc_3}\right)=\frac{1}{R_0}\frac{\Lambda c_4}{dc_3}>\frac{\Lambda c_4}{dc_3}$. Further from (3) and (4), we get $\overline{S}\le\frac{\Lambda c_4}{dc_3}$. Therefore, $\frac{\Lambda c_4}{dc_3}<\overline{S}\le\frac{\Lambda c_4}{dc_3}<\frac{\Lambda}{d}$, a contradiction. Hence $\overline{I_A}=0$ which implies $\lim_{t\to0}I_A(t)=0$. Since $\overline{I_A}=0$, $\overline{E}=0$ from (8) and (9), we get $d\overline{R}\le\epsilon\overline{I_S}\le\frac{\epsilon\delta_1}{c_5}\overline{I_A}=0$. Therefore, $\overline{R}=0$ and $\overline{I_S}=0$ which implies $\lim_{t\to0}R(t)=0$ and $\lim_{t\to0}I_S(t)=0$. Using Fluctuation lemma [70], we get a sequence $\rho_n\to\infty$ such that $S(\rho_n)\to\underline{S}$, $S'(\rho_n)\to0$, as $n\to\infty$. From (4), we get $S'(\rho_n)+c_6S(\rho_n)=\Lambda+\alpha_2L(\rho_n)$. Letting $n\to\infty$, we get $c_6\underline{S}=\Lambda+\alpha_2\underline{L}$ and from (5), we get $L'(\rho_n)+c_4L(\rho_n)=\alpha_1S(\rho_n)$ and then $c_4\underline{L}=\alpha_1\underline{S}$. Therefore, $c_6\underline{S}=\Lambda+\frac{\alpha_1\alpha_2}{c_4}\underline{S}$ which implies $\underline{S}=\frac{\Lambda c_4}{dc_3}$. But, $\overline{S}\le\frac{\Lambda c_4}{dc_3}=\underline{S}$. Hence, $\lim_{t\to0}S(t)=\frac{\Lambda c_4}{dc_3}$. Using $c_6\underline{S}=\Lambda+\alpha_2\underline{L}$ and $c_4\underline{L}=\alpha_1\underline{S}$, we get $\underline{L}=\frac{\Lambda\alpha_1}{dc_3}$. Further using (4) and (5), we get $\frac{c_6c_4\overline{L}}{\alpha_1}\le c_6\overline{S}\le\Lambda+\alpha_2\overline{L}$ which implies $\overline{L}\le\frac{\Lambda\alpha_1}{dc_3}$. So, $\overline{L}\le\frac{\Lambda\alpha_1}{dc_3}=\underline{L}$ and hence $\lim_{t\to0}L(t)=\frac{\Lambda\alpha_1}{dc_3}$. Therefore, $\lim_{t\to0}(S(t),L(t),E(t),I_A(t),I_S(t),R(t))=P_0$. □

7.2. Global stability of the EE

We now analyze the global stability of the endemic equilibrium (EE) of the system (1) using Lyapunov functional method [71].

Theorem 7. *The system (1) is globally asymptotically stable around the EE point $P_1(S^*,L^*,E^*,I_A^*,I_S^*)$, if $R_0>1$ and the following conditions are satisfied*

(i) $L^2L^*SS^{*2}(L^*S(S^*\alpha_1+L\alpha_2)^2-4LS^{*2}\alpha_1(L\alpha_2+\Lambda))<0$

(ii) $EE^*I_AL^2L^*S^{*2}\beta(L^*S(S^*\alpha_1+L\alpha_2)^2-4LS^{*2}\alpha_1(L\alpha_2+\Lambda))<0$

(iii) $E^2I_A^2L^2E^*L^*SS^{*2}(-2EI_ASE^*\beta)\gamma_1(SL^*(S^*\alpha_1+L\alpha_2)^2-4LS^{*2}\alpha_1(L\alpha_2+\Lambda))+E^2E^*\gamma_1^2(SL^*(S^*\alpha_1+L\alpha_2)^2-4LS^{*2}\alpha_1(L\alpha_2+\Lambda))+I_A^2S^2\beta^2(SE^*L^*(S^*\alpha_1+L\alpha_2)^2-4LS^{*2}\alpha_1(LE^*\alpha_2+EI_A^*S^*\beta+E^*\Lambda))>0$

(iv) $E^2I_A^2I_S^2L^2SE^*I_A^*I_S^*L^*S^2\delta_1(-2EI_AI_SE^*\beta\gamma_1(SL^*(S^*\alpha_1+L\alpha_2)^2-4LS^{*2}\alpha_1(L\alpha_2+\Lambda))+E^2I_SE^*\gamma_1^2(SL^*(S^*\alpha_1+L\alpha_2)^2-4LS^{*2}\alpha_1(L\alpha_2+\Lambda))+I_A^2S\beta(EI_S^*\delta_1(SL^*(S^*\alpha_1+L\alpha_2)^2-4LS^{*2}\alpha_1(L\alpha_2+\Lambda))+I_SS\beta(SE^*L^*(S^*\alpha_1+L\alpha_2)^2-4LS^{*2}\alpha_1(LE^*\alpha_2+EI_A^*S^*\beta+E^*\Lambda))))>0.$

Proof. Let us consider the Lyapunov functional $L:\Gamma\to\mathbb{R}^+$ as follows:

$$L(S,L,E,I_A,I_S)=a_1\int_{S^*}^{S}\left(\frac{m-S^*}{m}\right)dm+a_2\int_{L^*}^{L}\left(\frac{m-L^*}{m}\right)dm+a_3\int_{E^*}^{E}\left(\frac{m-E^*}{m}\right)dm+a_4\int_{I_A^*}^{I_A}\left(\frac{m-I_A^*}{m}\right)dm+a_5\int_{I_S^*}^{I_S}\left(\frac{m-I_S^*}{m}\right)dm \tag{10}$$

where $a_i\in\mathbb{R}^+(i=1,2,3,4,5)$ and their values are assumed in the following steps. Clearly $L(S,L,E,I_A,I_S)>0$ on $\Gamma-(S^*,L^*,E^*,I_A^*,I_S^*)$ and $L(S^*,L^*,E^*,I_A^*,I_S^*)=0$. Differentiating (10) with respect to time t, we get

$$\frac{dL}{dt}=a_1\left(\frac{S-S^*}{S}\right)\frac{dS}{dt}+a_2\left(\frac{L-L^*}{L}\right)\frac{dL}{dt}+a_3\left(\frac{E-E^*}{E}\right)\frac{dE}{dt}+a_4\left(\frac{I_A-I_A^*}{I_A}\right)\frac{dI_A}{dt}+a_5\left(\frac{I_S-I_S^*}{I_S}\right)\frac{dI_S}{dt} \tag{11}$$

We get the following result after some mathematical computations

$$\begin{aligned}\frac{dL}{dt}&=a_1(S-S^*)\left(-\frac{(\Lambda+\alpha_2L)(S-S^*)}{SS^*}+\frac{\alpha_2(L-L^*)}{S^*}-\beta(I_A-I_A^*)\right)\\&+a_2\alpha_1(L-L^*)\left(\frac{(S-S^*)}{L}-\frac{S^*(L-L^*)}{LL^*}\right)+a_3\beta(E-E^*)\left(\frac{S(I_A-I_A^*)}{E}-\frac{SI_A^*(E-E^*)}{EE^*}\right)\\&+a_4\gamma_1(I_A-I_A^*)\left(\frac{(E-E^*)}{I_A}-\frac{E^*(I_A-I_A^*)}{I_AI_A^*}\right)+a_5\delta_1(I_S-I_S^*)\left(\frac{(I_A-I_A^*)}{I_S}-\frac{I_A^*(I_S-I_S^*)}{I_SI_S^*}\right)\end{aligned} \tag{12}$$

$$\begin{aligned}\frac{dL}{dt}&=-\left(\frac{a_1(\Lambda+\alpha_2L)}{SS^*}\right)(S-S^*)^2-\left(\frac{a_2\alpha_1S^*}{LL^*}\right)(L-L^*)^2-\left(\frac{a_3\beta SI_A^*}{EE^*}\right)(E-E^*)^2\\&-\left(\frac{a_4\gamma_1E^*}{I_AI_A^*}\right)(I_A-I_A^*)^2-\left(\frac{a_5\delta_1I_A^*}{I_SI_S^*}\right)(I_S-I_S^*)^2+\left(\frac{a_1\alpha_2}{S^*}+\frac{a_2\alpha_1}{L}\right)(S-S^*)(L-L^*)\\&-a_1\beta(S-S^*)(I_A-I_A^*)+\left(\frac{a_3\beta S}{E}+\frac{a_4\gamma_1}{I_A}\right)(E-E^*)(I_A-I_A^*)+\left(\frac{a_5\delta_1}{I_S}\right)(I_A-I_A^*)(I_S-I_S^*).\end{aligned} \tag{13}$$

Eq. (13) is written as

$$\dot{L}=X^T\xi X \tag{14}$$

where

$$\xi=\begin{pmatrix}\xi_{11}&\xi_{12}&\xi_{13}&\xi_{14}&\xi_{15}\\\xi_{21}&\xi_{22}&\xi_{23}&\xi_{24}&\xi_{25}\\\xi_{31}&\xi_{32}&\xi_{33}&\xi_{34}&\xi_{35}\\\xi_{41}&\xi_{42}&\xi_{43}&\xi_{44}&\xi_{45}\\\xi_{51}&\xi_{52}&\xi_{53}&\xi_{54}&\xi_{55}\end{pmatrix},\text{ and }X=\begin{pmatrix}S-S^*\\L-L^*\\E-E^*\\I_A-I_A^*\\I_S-I_S^*\end{pmatrix}.$$

Here, $\xi=(\xi_{ij})_{1\le i,j\le5}$ is a real symmetric matrix with $\xi_{11}=-\frac{a_1(\Lambda+\alpha_2L)}{SS^*}$, $\xi_{12}=\frac{1}{2}\left(\frac{a_1\alpha_2}{S^*}+\frac{a_2\alpha_1}{L}\right)$, $\xi_{13}=0$, $\xi_{14}=-\frac{a_1\beta}{2}$, $\xi_{15}=0$, $\xi_{21}=\frac{1}{2}\left(\frac{a_1\alpha_2}{S^*}+\frac{a_2\alpha_1}{L}\right)$, $\xi_{22}=-\frac{a_2\alpha_1S^*}{LL^*}$, $\xi_{23}=0$, $\xi_{24}=0$, $\xi_{25}=0$, $\xi_{31}=0$, $\xi_{32}=0$, $\xi_{33}=\frac{-a_3\beta SI_A^*}{EE^*}$, $\xi_{34}=\frac{1}{2}\left(\frac{a_3\beta S}{E}+\frac{a_4\gamma_1}{I_A}\right)$, $\xi_{35}=0$, $\xi_{41}=-\frac{a_1\beta}{2}$, $\xi_{42}=0$, $\xi_{43}=\frac{1}{2}\left(\frac{a_3\beta S}{E}+\frac{a_4\gamma_1}{I_A}\right)$, $\xi_{44}=-\frac{a_4\gamma_1E^*}{I_AI_A^*}$, $\xi_{45}=\frac{1}{2}\left(\frac{a_5\delta_1}{I_S}\right)$, $\xi_{51}=0$, $\xi_{52}=0$, $\xi_{53}=0$, $\xi_{54}=\frac{1}{2}\left(\frac{a_5\delta_1}{I_S}\right)$, $\xi_{55}=-\frac{a_5\delta_1I_A^*}{I_SI_S^*}$.

The endemic equilibrium point P_1 would be globally asymptotically stable if $\dot{L}<0$, i.e., if the real quadratic form $X^T\xi X$ is negative definite. From Frobenius theorem [71], the real symmetric matrix ξ must be negative definite for the negativity of the quadratic form $X^T\xi X$ and hence must satisfy $(-1)^nD_n>0, n=1,2,3,4,5$, where

$$D_1=\xi_{11},\ D_2=\begin{vmatrix}\xi_{11}&\xi_{12}\\\xi_{21}&\xi_{22}\end{vmatrix},\ D_3=\begin{vmatrix}\xi_{11}&\xi_{12}&\xi_{13}\\\xi_{21}&\xi_{22}&\xi_{23}\\\xi_{31}&\xi_{32}&\xi_{33}\end{vmatrix},\ D_4=\begin{vmatrix}\xi_{11}&\xi_{12}&\xi_{13}&\xi_{14}\\\xi_{21}&\xi_{22}&\xi_{23}&\xi_{24}\\\xi_{31}&\xi_{32}&\xi_{33}&\xi_{34}\\\xi_{41}&\xi_{42}&\xi_{43}&\xi_{44}\end{vmatrix},\ D_5=|\xi|.$$

If we choose $a_i=1, i=1,2,3,4,5$, then we have the following conditions,

(i) $L^2L^*SS^{*2}(L^*S(S^*\alpha_1+L\alpha_2)^2-4LS^{*2}\alpha_1(L\alpha_2+\Lambda))<0$

(ii) $EE^*I_AL^2L^*S^{*2}\beta(L^*S(S^*\alpha_1+L\alpha_2)^2-4LS^{*2}\alpha_1(L\alpha_2+\Lambda))<0$

(iii) $E^2I_A^2L^2E^*L^*SS^{*2}(-2EI_ASE^*\beta)\gamma_1(SL^*(S^*\alpha_1+L\alpha_2)^2-4LS^{*2}\alpha_1(L\alpha_2+\Lambda))+E^2E^*\gamma_1^2(SL^*(S^*\alpha_1+L\alpha_2)^2-4LS^{*2}\alpha_1(L\alpha_2+\Lambda))+I_A^2S^2\beta^2(SE^*L^*(S^*\alpha_1+L\alpha_2)^2-4LS^{*2}\alpha_1(LE^*\alpha_2+EI_A^*S^*\beta+E^*\Lambda))>0$

(iv) $E^2 I_A^2 I_S^2 L^2 S E^* I_A^* I_S^* L^* S^2 \delta_1(-2EI_A I_S SE^*\beta\gamma_1(SL^*(S^*\alpha_1+L\alpha_2)^2-4LS^{*2}\alpha_1(L\alpha_2+\Lambda))+E^2 I_S E^*\gamma_1^2(SL^*(S^*\alpha_1+L\alpha_2)^2-4LS^{*2}\alpha_1(L\alpha_2+\Lambda))+I_A^2 S\beta(EI_S^*\delta_1(SL^*(S^*\alpha_1+L\alpha_2)^2-4LS^{*2}\alpha_1(L\alpha_2+\Lambda))+I_S S\beta(SE^*L^*(S^*\alpha_1+L\alpha_2)^2-4LS^{*2}\alpha_1(LE^*\alpha_2+EI_A^*S^*\beta+E^*\Lambda)))) > 0$ □

8. Dynamics of the system with control after lockdown

In this section, an optimal control system based on the CoV SARS-2 pandemic model (1) has been set up so that this vulnerable situation can be normalized. Here, we introduce three optimal control variables $v_1(t)$, $v_2(t)$ and $v_3(t)$. The optimal control $v_1(t)$ represents the vaccination on exposed population per unit time at t, the control $v_2(t)$ represents the recovery rate of the asymptomatic infected individuals under treatment per unit time at t, and the control $v_3(t)$ represents the recovery rate of the symptomatic infected individual under treatment per unit time at t. Then, the pandemic model with vaccine and treatments after lockdown becomes:

$$\begin{cases} \frac{dS}{dt} &= \Lambda - \beta S I_A - dS \\ \frac{dE}{dt} &= \beta S I_A - \left(\gamma_1+\gamma_2+d+v_1(t)\right)E \\ \frac{dI_A}{dt} &= \gamma_1 E - \left(\delta_1+\delta_2+\mu_1+d+v_2(t)\right)I_A \\ \frac{dI_S}{dt} &= \delta_1 I_A - \left(d+\mu_2+\epsilon+v_3(t)\right)I_S \\ \frac{dR}{dt} &= (\gamma_2+v_1(t))E + (\delta_2+v_2(t))I_A + (\epsilon+v_3(t))I_S - dR \end{cases} \tag{15}$$

satisfying the initial conditions

$$S(0)=S_0, E(0)=E_0, I_A(0)=I_{A_0}, I_S(0)=I_{S_0}, R(0)=R_0 \geq 0 \tag{16}$$

The effect of infection on exposed, asymptomatic and symptomatic infected phases are negative for recovered individuals around them. Thus it is essential to minimize them.

The objective functional [72–76] is defined as

$$J(v_1(t),v_2(t),v_3(t)) = \int_0^{t_e}\left[W_1E(t)+W_2I_A(t)+W_3I_S(t)+\frac{W_4}{2}v_1^2(t)+\frac{W_5}{2}v_2^2(t)+\frac{W_6}{2}v_3^2(t)\right]dt \tag{17}$$

where W_i $(i=1,2,3,4,5,6)$ are positive weight factors that balance the size of the terms in the integrand. The weights W_4, W_5, W_6 represents the human's level of acceptance of the vaccination, treatments on asymptotic and symptomatic infected population respectively. Here, $E(t)$, $I_A(t)$ and $I_S(t)$ are the state variables with the admissible control set $V=\{(v_1,v_2,v_3) : v_i \text{ is measurable}, 0 \leq v_i \leq 1,\ t \in [0,t_e],\ \text{for } i=1,2,3\}$ and we have to seek the optimal control (v_1^*,v_2^*,v_3^*) such that the objective functional is to be minimized, i.e., $J(v_1^*,v_2^*,v_3^*) = \min\{\ J(v_1,v_2,v_3) : (v_1,v_2,v_3) \in V\}$.

8.1. Existence of an optimal control

Here, we shall show that there exists an optimal control (v_1^*,v_2^*,v_3^*) for the control system (15) with initial condition (16). Let $E(t)$, $I_A(t)$ and $I_S(t)$ be the state variables with controls $v_1(t)$, $v_2(t)$ and $v_3(t)$ respectively.

Theorem 8. *For the control system (15) with initial condition (16), there exists an optimal control (v_1^*,v_2^*,v_3^*) such that $J(v_1^*,v_2^*,v_3^*) = \min\{J(v_1,v_2,v_3) :\ (v_1,v_2,v_3) \in V\}$.*

Proof. The optimal control system (16) can be expressed as the following form:

$$G(\phi) = C\phi + F(\phi) \tag{18}$$

where

$$G(\phi)=\begin{bmatrix}\dot{S}(t)\\ \dot{E}(t)\\ \dot{I}_A(t)\\ \dot{I}_S(t)\\ \dot{R}(t)\end{bmatrix},\quad \phi=\begin{bmatrix}S(t)\\ E(t)\\ I_A(t)\\ I_S(t)\\ R(t)\end{bmatrix},\quad F(\phi)=\begin{bmatrix}\Lambda-\beta S(t)I_A(t)\\ \beta S(t)I_A(t)\\ 0\\ 0\\ 0\end{bmatrix},$$

and

$$C=\begin{bmatrix}-d & 0 & 0 & 0 & 0\\ 0 & -(\gamma_1+\gamma_2+d+v_1) & 0 & 0 & 0\\ 0 & \gamma_1 & -(\delta_1+\delta_2+\mu_1+d+v_2) & 0 & 0\\ 0 & 0 & \delta_1 & -(d+\mu_2+\epsilon+v_3) & 0\\ 0 & (\gamma_2+v_1) & (\delta_2+v_2) & (\epsilon+v_3) & -d\end{bmatrix}$$

Now,

$$\left|F(\phi_1)-F(\phi_2)\right| \leq p_1\left|S_1(t)-S_2(t)\right| + p_2\left|I_{A_1}(t)-I_{A_2}(t)\right|,$$

where the constants $p_1>0$ and $p_2>0$ are independent of the variables $S(t)$ and $I_A(t)$.

Hence,

$$\left|G(\phi_1) - G(\phi_2)\right| \leq C\left|\phi_1 - \phi_2\right| + \left|F(\phi_1) - F(\phi_2)\right| \leq p\left|\phi_1 - \phi_2\right| < \infty$$

where $p = p_1 + p_2 + \|C\| < \infty$. Therefore, $G(\phi)$ is said to be uniformly Lipschitz continuous function. From the definition of V and restriction on $S(t), E(t), I_A(t), I_S(t), R(t) \geq 0$, we can say that a solution of the system (18) exist [65]. In this case, all the state variables and control variables are non-negative. The convexity [76] of $J(v_1(t), v_2(t), v_3(t))$ (in Equ. (17)) is satisfied in the minimizing optimal control problem (15). As the set of control variable $(v_1, v_2, v_3) \in V$ is closed and convex, the system of optimal control is bounded [77] which determines the compactness required for the existence of the optimal control (v_1^*, v_2^*, v_3^*). Again, we observed that the integrand of (17) i.e., $W_1E(t) + W_2I_A(t) + W_3I_S(t) + \frac{W_4}{2}v_1^2(t) + \frac{W_5}{2}v_2^2(t) + \frac{W_6}{2}v_3^2(t)$ is convex on the control set V. Since the state variables are bounded, $\exists\ n > 1$ and positive real numbers k_1 and k_2 such than $J(v_1, v_2, v_3) \geq k_1 + k_2(|v_1|^2 + |v_2|^2 + |v_3|^2)^{\frac{n}{2}}$, which shows the existence of an optimal control. □

8.2. Depiction of the optimal controls

To describe the necessary conditions for the optimal control variables, the Pontryagin's maximum principle [78] is applied and it follows the Hamiltonian (H) as the form:

$$\begin{aligned} H = {} & \left(W_1E + W_2I_A + W_3I_S + \frac{W_4}{2}v_1^2 + \frac{W_5}{2}v_2^2 + \frac{W_6}{2}v_3^2\right) + \tau_1[\Lambda - \beta SI_A - dS] \\ & + \tau_2[\beta SI_A - (\gamma_1 + \gamma_2 + d + v_1)E] + \tau_3[\gamma_1 E - (\delta_1 + \delta_2 + \mu_1 + d + v_2)I_A] \\ & + \tau_4[\delta_1 I_A - (d + \mu_2 + \epsilon + v_3)I_S] + \tau_5[(\gamma_2 + v_1)E + (\delta_2 + v_2)I_A + (\epsilon + v_3)I_S - dR] \end{aligned} \tag{19}$$

where $\tau_i(t),\ i = 1, 2, 3, 4, 5$, are the adjoint functions to be determined duly.

Theorem 9. *Let $S^*(t), E^*(t), I_A^*(t), I_S^*(t)$ and $R^*(t)$ are optimal solutions for the optimal control problem (15) with initial conditions (16) associated with the optimal control variables $v_1^*(t),\ v_2^*(t)$ and $v_3^*(t)$. Then there exist five ad-joint variables $\tau_1, \tau_2, \tau_3, \tau_4$ and τ_5 which satisfy*

$$\begin{aligned} \tau_1' &= (\tau_1 - \tau_2)\beta I_A^*(t) + \tau_1 d \\ \tau_2' &= -W_1 + (\tau_2 - \tau_3)\gamma_1 + (\tau_2 - \tau_5)(\gamma_2 + v_1) + d\tau_2 \\ \tau_3' &= -W_2 + (\tau_1 - \tau_2)\beta S^*(t) + (\tau_3 - \tau_4)\delta_1 + (\tau_3 - \tau_5)(\delta_2 + v_2) - \tau_3(d + \mu_1) \\ \tau_4' &= -W_3 + (\tau_4 - \tau_5)(\epsilon + v_3) + \tau_4(d + \mu_2) \\ \tau_5' &= \tau_5 d \end{aligned} \tag{20}$$

with the transversality conditions

$$\tau_i(t_e) = 0 \quad \textit{for all } i = 1 \textit{ to } 5. \tag{21}$$

Furthermore, the solutions of optimal control variables are given as follows:

$$v_1^* = min\left\{max\left\{0, \frac{(\tau_2 - \tau_5)E^*(t)}{W_4}\right\}, 1\right\} \tag{22}$$

$$v_2^* = min\left\{max\left\{0, \frac{(\tau_3 - \tau_5)I_A^*(t)}{W_5}\right\}, 1\right\} \tag{23}$$

$$v_3^* = min\left\{max\left\{0, \frac{(\tau_4 - \tau_5)I_S^*(t)}{W_6}\right\}, 1\right\} \tag{24}$$

Proof. To determine the all five ad-joint functions and the transversality conditions, Hamiltonian (19) has been used. After setting $S(t) = S^*(t), E(t) = E^*(t), I_A = I_A^*(t), I_S = I_S^*(t)$ and $R(t) = R^*(t)$ and differentiating the Hamiltonian (19) with respect to S, E, I_A, I_S and R, we obtain Eqs. (20). From the Pontryagin's Maximum Principle [78], we obtained the following optimality condition:

$$\frac{\partial H}{\partial v_i} = W_{(i+3)}v_i^* - (\tau_{(i+1)} - \tau_5)O_i = 0 \quad \text{at} \quad v_i = v_i^* \quad \text{for } i = 1, 2, 3.$$

where $O_1 = E^*(t), O_2 = I_A^*(t), O_3 = I_S^*(t)$.

Using the bounds for the controls v_i $(i = 1, 2, 3)$, it is obtained that

$$v_i^* = \begin{cases} \frac{(\tau_{(i+1)} - \tau_5)O_i}{W_{(i+3)}} & , \text{ if } \ 0 \leq \frac{(\tau_{(i+1)} - \tau_5)O_i}{W_{(i+3)}} \leq 1 \\ 0 & , \text{ if } \ \frac{(\tau_{(i+1)} - \tau_5)O_i}{W_{(i+3)}} \leq 0 \\ 1 & , \text{ if } \ \frac{(\tau_{(i+1)} - \tau_5)O_i}{W_{(i+3)}} \geq 1 \end{cases}$$

$$\text{or,} \quad v_i^* = min\left\{max\left\{0, \frac{(\tau_{(i+1)} - \tau_5)O_i}{W_{(i+3)}}\right\}, 1\right\}, \quad \text{for} \quad i = 1, 2, 3,$$

which represents the ultimate result of (22)–(24). □

The solution of the optimal control variables $(\upsilon_1^*, \upsilon_2^*, \upsilon_3^*)$ is given by Eqs. (22)–(24). The optimal control and the state variables are obtained after solving the optimality system consisting of the state system (15)), the adjoint system (20), initial condition (16), the transversality condition (21) and the characterization of the optimal control (22)–(24). Further it is noticed that the second derivative of the integrand of J from ((17) with respect to the control variables υ_1, υ_2 and υ_2 is positive, which guarantees that the optimal problem is minimum at the controls υ_1^*, υ_2^*, υ_2^*. Substituting the optimal control values υ_1^*, υ_2^*, υ_2^* in the control system (15), we find the system as follows

$$\begin{aligned}
\frac{dS^*}{dt} &= \Lambda - \beta S^* I_A^* - dS^* \\
\frac{dE^*}{dt} &= \beta S^* I_A^* - (\gamma_1 + \gamma_2 + d)E^* - \left[min\left\{ max\left\{ 0, \frac{(\tau_2 - \tau_5)E^*}{W_4} \right\}, 1 \right\}\right] E^* \\
\frac{dI_A^*}{dt} &= \gamma_1 E^* - (\delta_1 + \delta_2 + \mu_1 + d)I_A^* - \left[min\left\{ max\left\{ 0, \frac{(\tau_3 - \tau_5)I_A^*}{W_5} \right\}, 1 \right\}\right] I_A^* \\
\frac{dI_S^*}{dt} &= \delta_1 I_A^* - (d + \mu_2 + \epsilon)I_S^* - \left[min\left\{ max\left\{ 0, \frac{(\tau_4 - \tau_5)I_S^*}{W_6} \right\}, 1 \right\}\right] I_S^* \\
\frac{dR^*}{dt} &= (\gamma_2 E^* + \delta_2 I_A^* + \epsilon I_S^*) - dR^* + \left[min\left\{ max\left\{ 0, \frac{(\tau_2 - \tau_5)E^*}{W_4} \right\}, 1 \right\}\right] E^* \\
&\quad + \left[min\left\{ max\left\{ 0, \frac{(\tau_3 - \tau_5)I_A^*}{W_5} \right\}, 1 \right\}\right] I_A^* + \left[min\left\{ max\left\{ 0, \frac{(\tau_4 - \tau_5)I_S^*}{W_6} \right\}, 1 \right\}\right] I_S^*
\end{aligned} \tag{25}$$

and the Hamiltonian (19) can be rewritten as follows

$$\begin{aligned}
H^* &= W_1 E^* + W_2 I_A^* + W_3 I_S^* + \frac{1}{2}\left[W_4 \left(min\left\{ max\left\{ 0, \frac{(\tau_2 - \tau_5)E^*}{W_4} \right\}, 1 \right\}\right)^2 \right. \\
&\quad + W_5 \left(min\left\{ max\left\{ 0, \frac{(\tau_3 - \tau_5)I_A^*}{W_5} \right\}, 1 \right\}\right)^2 + W_6 \left(min\left\{ max\left\{ 0, \frac{(\tau_4 - \tau_5)I_S^*}{W_6} \right\}, 1 \right\}\right)^2 \left. \right] \\
&\quad + \tau_1(t)\frac{dS^*}{dt} + \tau_2(t)\frac{dE^*}{dt} + \tau_3(t)\frac{dI_A^*}{dt} + \tau_4(t)\frac{dI_S^*}{dt} + \tau_5(t)\frac{dR^*}{dt}.
\end{aligned} \tag{26}$$

To determine the optimal control and state variables, it is required to solve the system (25) and (26) numerically.

9. Numerical simulation

Parameter estimations: This part presents the estimation procedure of various parameters in the proposed model. The well-known non-linear least square curve fitting technique is used for this purpose. The confirmed infected cases in India from 23rd March to 31st December 2020 is taken in the estimation process. The Parameter estimation and fixing the initial values for each population class are difficult due to lack of information. We assume that the total population of India is approximately 135 crores. We divide this total Indian population into different classes following the COVID-19 situation of India. The number of susceptible population (S) and lockdown population (L) are not known precisely. Fixing the initial value for the exposed (E) class and asymptomatic infected (I_A) class is challenging in epidemic models. Only the information of symptomatic infected (I_S) class is available, and hence except for the symptomatic infected (I_S) class, the initial values of all other classes are assumed hypothetically based on the COVID-19 situation of India. The total population of India is approximately 135 crores, and the number of human births per day is approximately 70,000. The Life expectancy in India is approximately 68 years. Therefore it is assumed that $\Lambda = 70000$ and $d = \frac{1}{68\times356} = 0.00004$. The values of the parameters $\alpha_1, \alpha_2, \beta, \mu_1, \mu_2$ are best fitted due to the unavailability of accurate information. The parameter values are chosen based on the characteristics of COVID-19 disease in India. In the proposed model, it is assumed that some percentage of the exposed population are recovered from the infection with in 10 days due to low virus load, which is considered as the observation period of some individuals in the exposed population and hence it is assumed that $\gamma_2 = \frac{1}{10} = 0.1$. For best fitting, we assume that $\gamma_2 = 0.101$. The incubation period for the coronavirus is between two and fourteen days after an effective contact with the asymptomatic infected individuals of this COVID-19 disease. A report published earlier in the pandemic period states that more than 97% of people who contract SARS-CoV-2 show symptoms within 12 days after having effective contact with the asymptomatic infected individuals. It appears that transmission can occur between one to three days before any symptoms appear. So, we assume some individuals move from exposed class (E) to asymptomatic infected (I_A) class within eight days. Therefore $\gamma_1 = \frac{1}{8} = 0.125$. Those with a mild case of COVID-19 infection usually recover between one to two weeks. Recovery can take six weeks or more for severe cases where the vital organs like the heart, kidneys, lungs and brain are damaged. So, we assume that some individuals of the asymptomatic infected (I_A) class move to the recovered class within twelve days and hence it is assumed that $\delta_2 = \frac{1}{12} = 0.08$. In our model, the symptomatic case means the confirmed infected cases tested and declared by the Government. The COVID-19 testing process takes between two to three days, and not all infected people are tested due to a lack of infrastructure and hence considering all these factors, we assume that some percentage of individuals move from asymptomatic infected (I_A) class to symptomatic infected (I_S) class within six days. Therefore $\delta_1 = \frac{1}{6} = 0.17$. We assume that the recovery time for symptomatic infected (I_S) class is 13 days and hence $\epsilon = \frac{1}{13} = 0.077$.

Analytical works can never be completed without numerical simulation results. Here, firstly we consider the cases when R_0 value is less than unity using the parameter values $\Lambda = 6\times10^4, \alpha_1 = 5\times10^{-3}, \alpha_2 = 10\times10^{-4}, \beta = 7\times10^{-10}, \gamma_1 = 8\times10^{-2}, \gamma_2 = 5\times10^{-2}, \delta_1 = 7.5\times10^{-2}, \delta_2 = 5\times10^{-2}, \mu_1 = 10\times10^{-5}, \mu_2 = 10\times10^{-4}, d = 4\times10^{-5}, \epsilon = 7\times10^{-2}$. Using these values for various

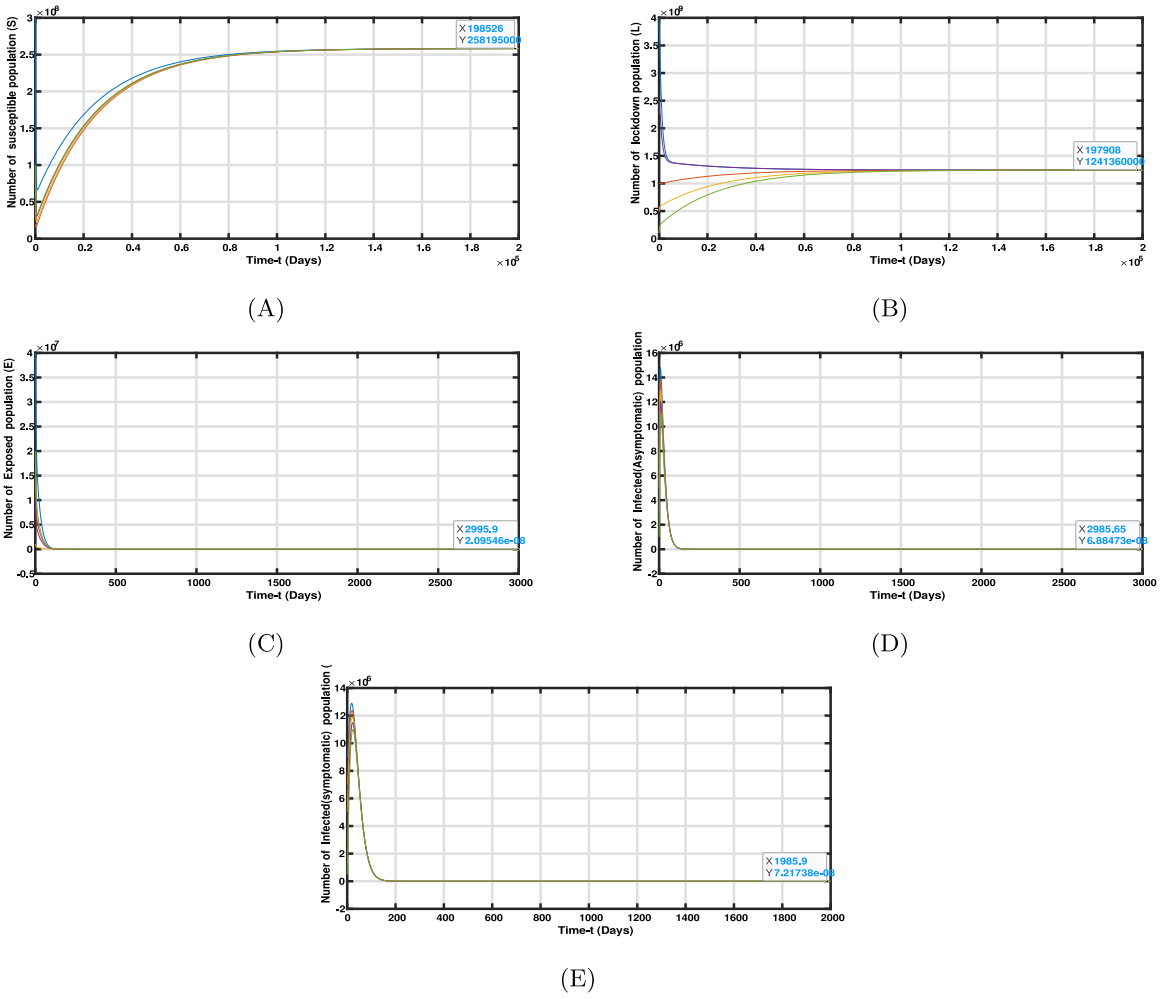

Fig. 2. The time series plot of (A) susceptible phase, (B) lockdown phase, (C) exposed phase, (D) asymptomatic infected phase and (E) symptomatic infected phase with various initial conditions when $R_0 = 0.89 < 1$.

initial conditions, the model's dynamics are analyzed and presented in Figs. 2(A)-2(E). These figures clearly shows that when $R_0 = 0.89 < 1$, the susceptible population(S) and lockdown population(L) persists but the exposed population(E), asymptomatic infected population(I_A) and symptomatic infected population(I_S) tends to zero as t $\to \infty$, i.e., the system approaches the disease free equilibrium $P_0(2.58278 \times 10^8, 1.24172 \times 10^9, 0, 0, 0)$ in long run. These numerical results supports the results of Theorem 4.

Next, we consider the case when $R_0 = 1.75 > 1$, using the parameter values $\Lambda = 6 \times 10^4, \alpha_1 = 5 \times 10^{-3}, \alpha_2 = 10 \times 10^{-4}, \beta = 7{\times}10^{-10}, \gamma_1 = 8{\times}10^{-2}, \gamma_2 = 5{\times}10^{-2}, \delta_1 = 7.5{\times}10^{-2}, \delta_2 = 5{\times}10^{-2}, \mu_1 = 10{\times}10^{-5}, \mu_2 = 10{\times}10^{-4}, d = 2{\times}10^{-5}, \epsilon = 7{\times}10^{-2}$ for various initial conditions, the dynamics of the model is presented in Figs. 3(A)-3(E). These figures clearly shows that the susceptible population(S), lockdown population(L), exposed population(E), asymptomatic infected population(I_A) and symptomatic infected population(I_S) persists as t $\to \infty$, i.e., the system approaches the endemic equilibrium $P_1(2.91 \times 10^8, 1.42 \times 10^9, 1.98 \times 10^5, 1.26 \times 10^5, 1.34 \times 10^5)$ in long run.

The behavior of the parameters α_1, α_2 and β with respect to R_0 is presented through Figs. 4(A)-4(C). From Fig. 4(A), it is clear that when the progression rate from the susceptible class to the lockdown class increases, the basic reproduction number (R_0) decreases and goes below one. So, the system approaches the DFE P_0, which is globally stable. Hence, the more the population is in lockdown, the more likely it is that the disease will become extinct.

From Fig. 4(B), it is clear that as the progression rate from lockdown class to susceptible class increases, the basic reproduction number (R_0) increases steadily and goes over unity and, as a result, endemic equilibrium is stable. Hence, if lockdown is not strictly enforced, the disease persists in society for a long time.

From Fig. 4(C), it is obvious that as the effective contact rate of asymptomatic infective individuals increases the basic reproduction number (R_0) increases steadily and goes over-unity hence the endemic equilibrium is stable and the disease persists in society for a long period.

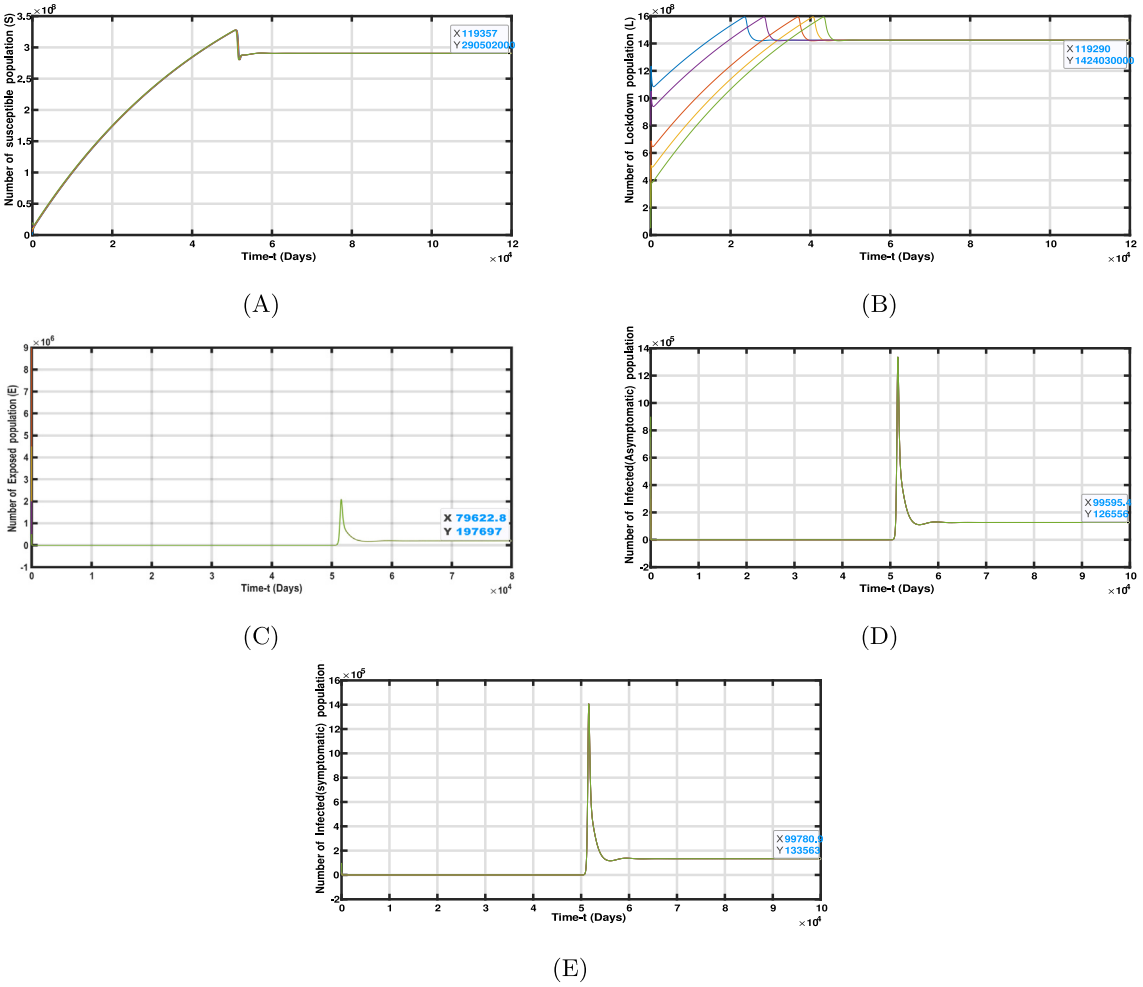

Fig. 3. The time series plot of (A) susceptible phase, (B) lockdown phase, (C) exposed phase, (D) asymptomatic infected phase and (E) symptomatic infected phase with various initial conditions when $R_0 = 1.75 > 1$.

Table 2
The actual field value of all parameters.

Parameter	Value per day
Λ	7×10^{4}
α_1	53×10^{-4}
α_2	10×10^{-4}
β	121×10^{-11}
γ_1	125×10^{-3}
γ_2	101×10^{-3}
δ_1	17×10^{-2}
δ_2	8×10^{-2}
μ_1	10×10^{-5}
μ_2	11×10^{-4}
d	4×10^{-5}
ϵ	77×10^{-3}

In Figs. 5 and 6, the analysis is made on the change of R_0 with respect to α_1 and α_2, α_1 and β, α_2 and β respectively, fixing other all parameter values as in Table 2. It is seen in Figs. 5(A) and 6(A) that as α_2 increases, R_0 increases sharply, exceeding unity, thus stabilizing endemic equilibrium. As a result, the disease persists in society for a long time. With Figs. 5(B) and 6(B), it is apparent that as β, the effective contact rate of infected individuals, rises, R_0 value rises in proportion exceeding unity, thereby maintaining the stability of endemic equilibrium, which ensures that the disease persists in society. From Fig. 5(C) and Fig. 6(C), it is obvious that as α_2 which is the progression rate from lockdown class to susceptible class, increases, there is a high chance of individuals in

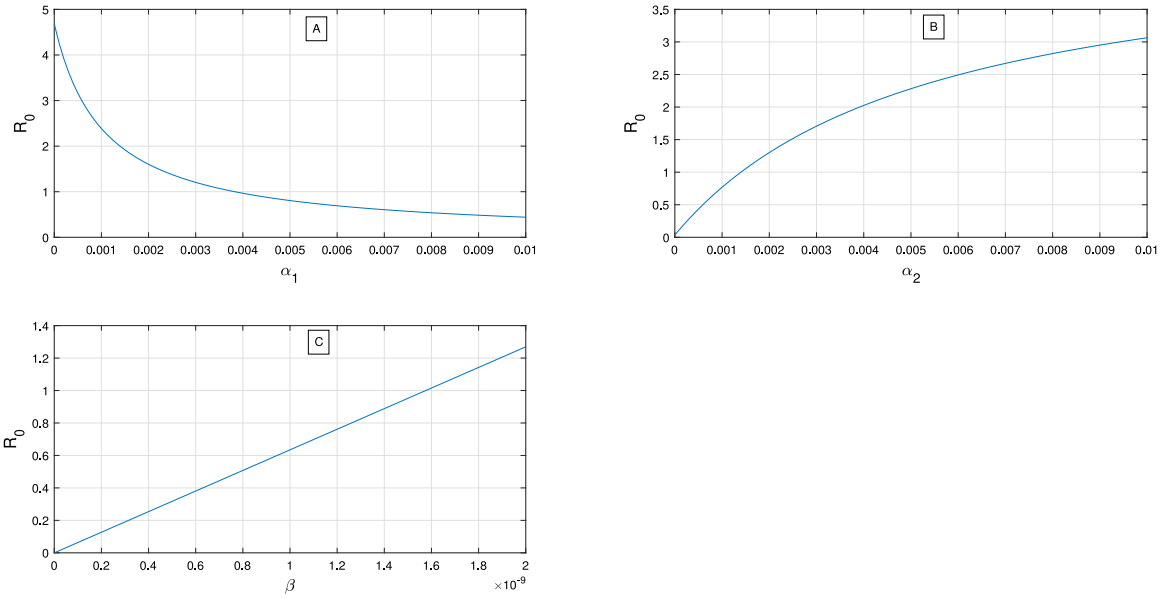

Fig. 4. Sensitivity analysis of R_0: (A) based on α_1, (B) based on α_2 and (C) based on β_1.

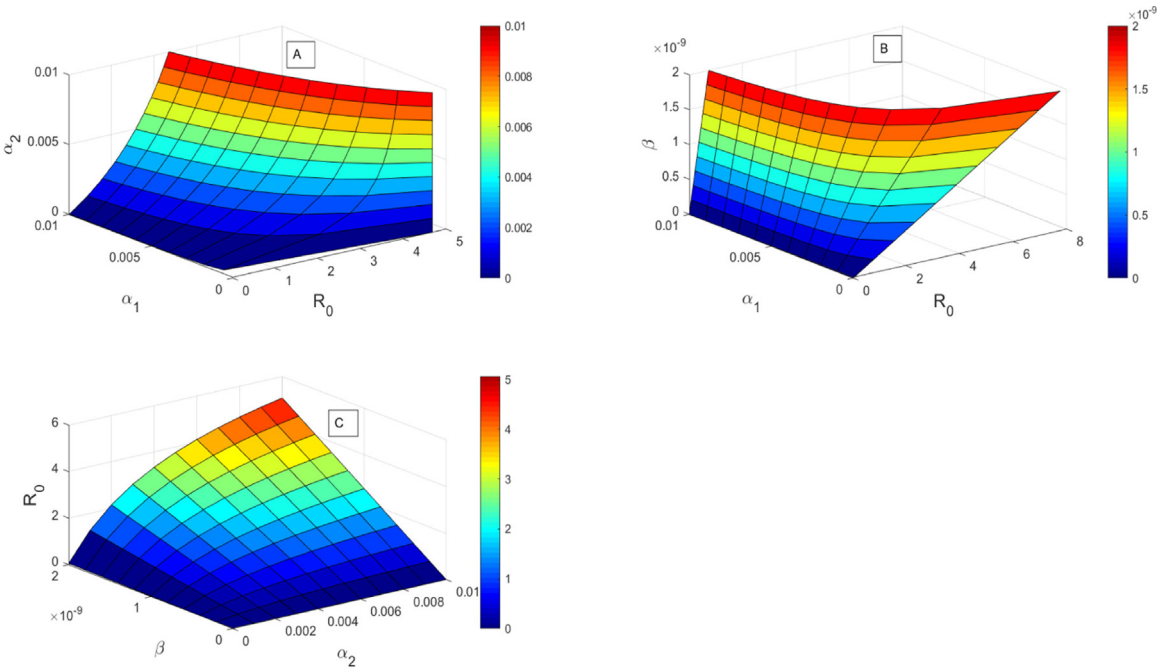

Fig. 5. (A) Change of R_0 based on α_1 and α_2; (B) Change of R_0 based on α_1 and β; and (C) Change of R_0 based on α_2 and β.

susceptible compartment getting in contact with asymptomatic infective individuals, which is represented by the effective contact rate β also increases and as a result, the R_0 value exceeds unity. Hence there is a wide spread of the disease in the society.

Figs. 7–8 shows the time-series graph (based on days) of the symptomatic infected population and the total death within a time period. In Figs. 9(A)–9(D), we studied the long-run history of the susceptible, exposed, locked down and asymptomatic infected classes of the model for different degrees of lockdown. In Figs. 10(A)–10(D), we studied the long-run history of the susceptible, exposed, locked down and asymptomatic infected classes of the model for various values of the effective contact rate of asymptomatic infected individuals β. In Figs. 11–13, we illustrate the optimal control strategies.

Fig. 7 shows the time history of the symptomatic infected population and the total death population for $\alpha_1 = 0.0052$; $\alpha_1 = 0.0053$; and $\alpha_1 = 0.0054$ with parameter values and initial population size as given in Table 2 and Table 3 respectively, for the period 23rd

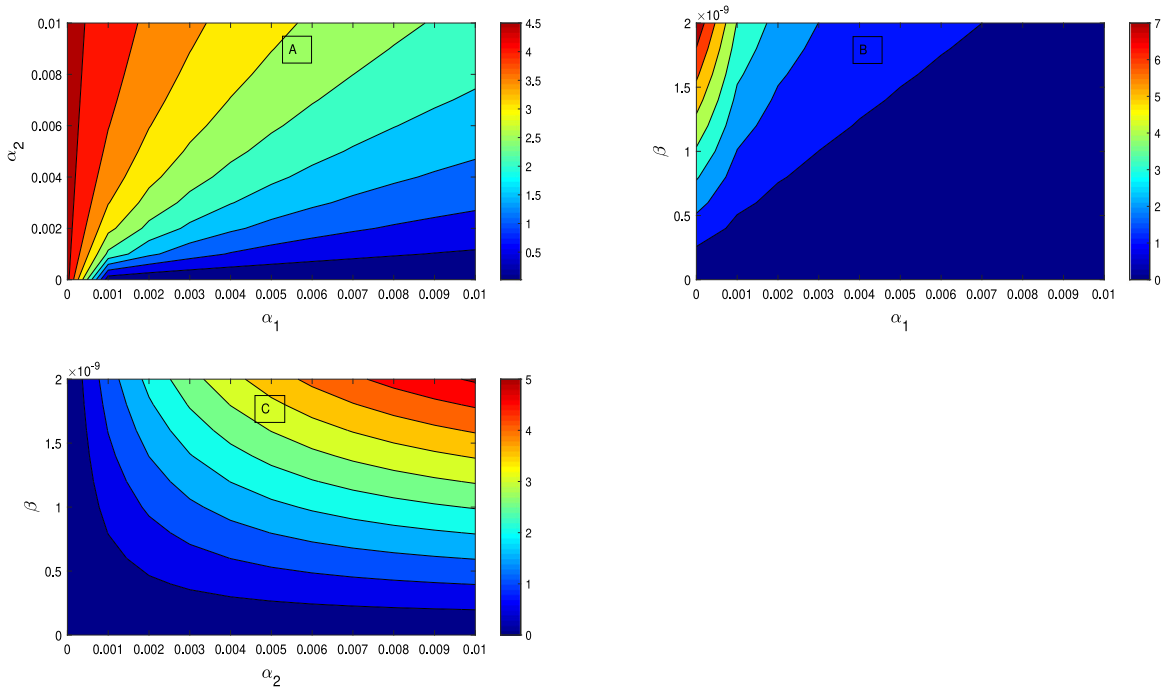

Fig. 6. Contour plots of (A) R_0 based on α_1 and α_2, (B) R_0 based on α_1 and β, (C) R_0 based on α_2 and β.

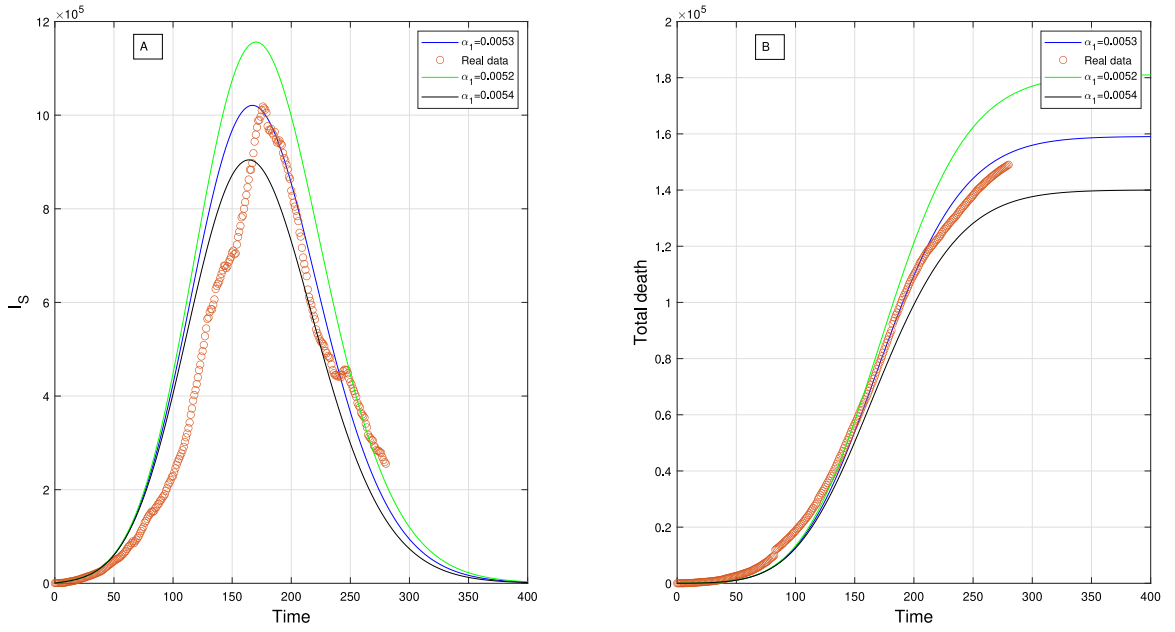

Fig. 7. Time history of the symptomatic infected population (I_S) and the total death for different values of α_1.

March to 31st December, 2020. In Fig. 7, it is depicted that the real data of the total infected almost coincide with our proposed model curve from 23rd March to 31st December, 2020. It is seen that, the proposed epidemic model is best fitted to the current situation of India. Fig. 7 clearly show that lockdown parameter α_1 has an apparent effect in controlling the spread of the disease in society.

Fig. 8 shows the time history of the total infected and the total death for $\beta = 0.00000000120$; $\beta = 0.00000000121$; and $\beta = 0.00000000122$ with parameter values and initial conditions are given in Table 2 and Table 3 respectively, for the period 23rd March to 31st December, 2020. It is seen that, the proposed epidemic model fits well according the present situation in India.

Table 3
Initial population size.

$S(0)$	$L(0)$	$E(0)$	$I_A(0)$	$I_S(0)$	$R(0)$
650000000	700000000	6000	2000	455	2000

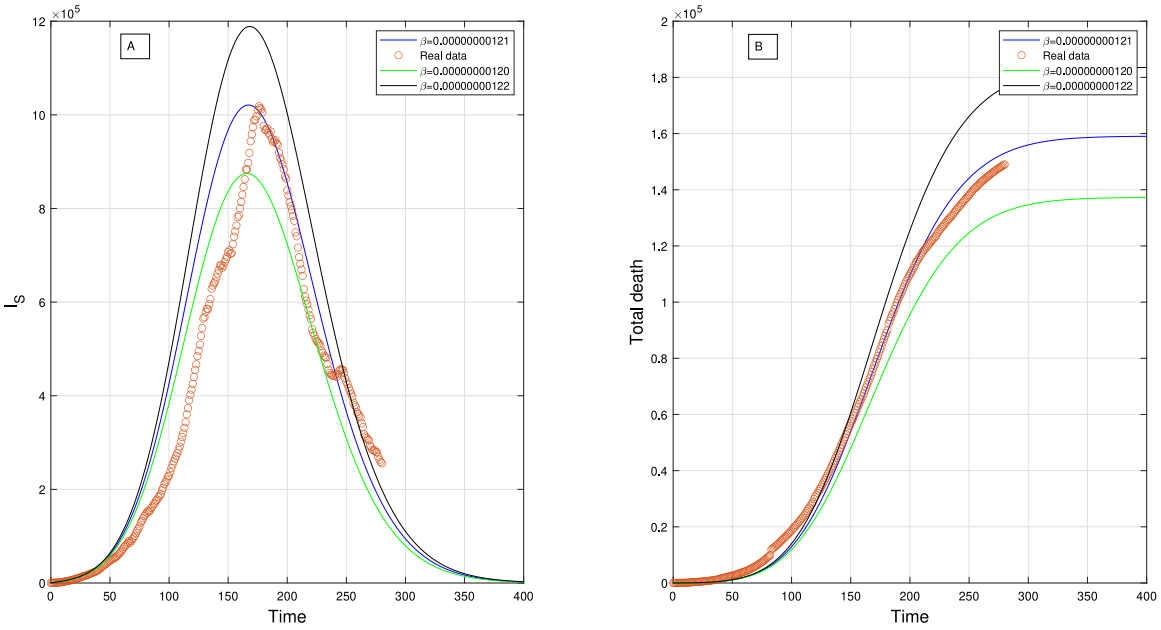

Fig. 8. Time history of the symptomatic infected population (I_S) and the total death for different value of β.

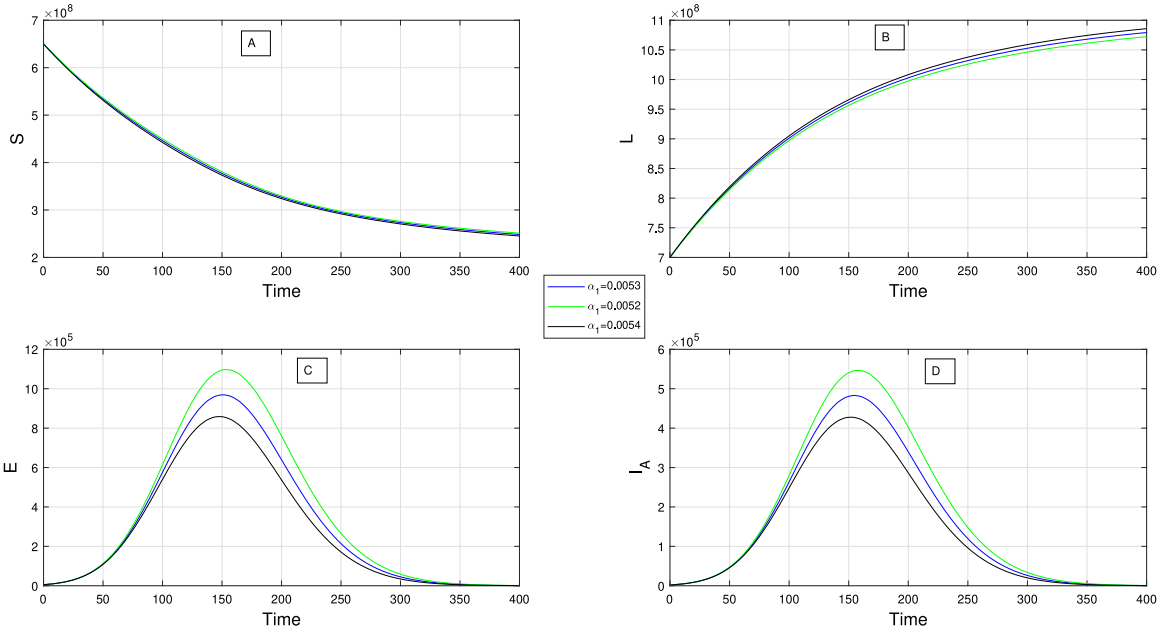

Fig. 9. Long time history of each compartment for different value of α_1.

It can be seen from Fig. 8(A) that the number of symptomatic infected individuals increases as the effective contact rate of the asymptomatic infected individuals (β) increases.

Figs. 9(A)-9(D) shows the long-run history of the susceptible, exposed, lockdown, and asymptotic infected classes of the proposed epidemic model for different values of the lockdown parameter α_1. Figs. 9(C) and 9(D) show that as the value of α_1 increases, the

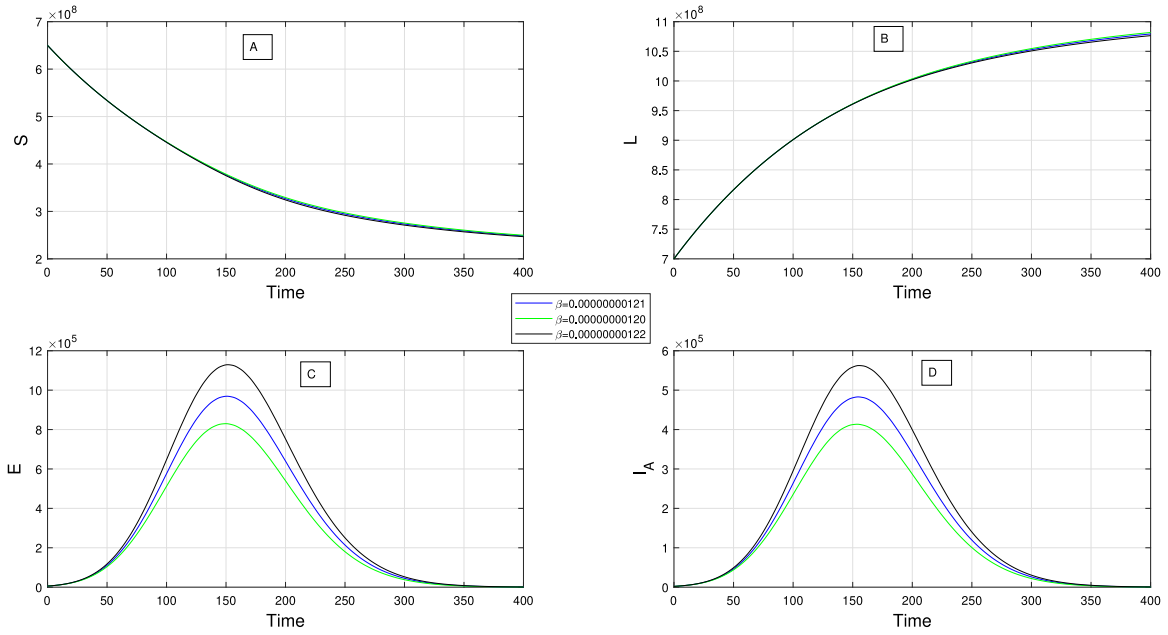

Fig. 10. Long time history of each compartment for different value of β.

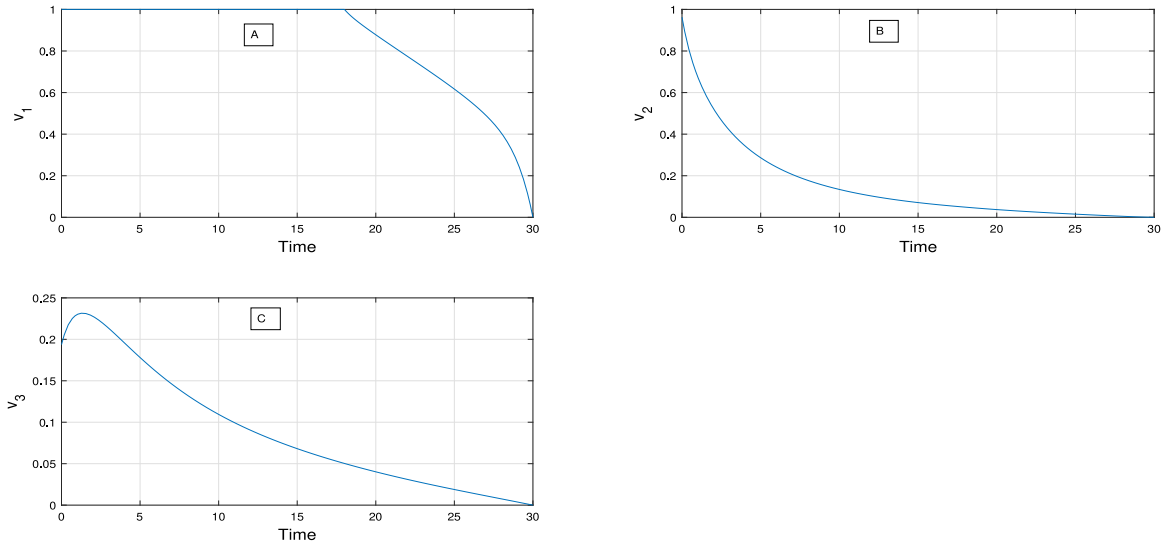

Fig. 11. The optimal control diagrams for the three controls, namely (A) vaccination control $v_1(t)$ on E, (B) the treatment control $v_2(t)$ on I_A and (C) the treatment control $v_3(t)$ on I_S.

number of exposed and therefore asymptomatic infected populations is reduced. Therefore, the spread of the disease in society is also reduced. These figures clearly demonstrated the importance of the lockdown in controlling the spread of the disease.

Figs. 10(A)-10(D) shows the long-run history of the susceptible, exposed, lockdown, and asymptotic infected classes of the proposed epidemic model for different values of the effective contact rate of asymptomatic infected individuals (β). Figs. 10(C) and 10(D) show that as the value of β increases, the number of exposed and therefore asymptomatic infected populations is increased. This paves way for the rapid spread of the disease in society. These figures clearly demonstrated the importance of the avoiding direct contact with asymptomatic infected individuals and hence the rapid spread of the disease in society is drastically reduced.

For numerical analysis of the optimal problem (15), the positive weights are taken as $W_1 = 10 \times 10^3; W_2 = 10 \times 10^3; W_3 = 10 \times 10^3; W_4 = 5 \times 10^8; W_5 = 5 \times 10^{10}; W_6 = 5 \times 10^{10}$; and initial population as $S(0) = 1.3446 \times 10^9; E(0) = 30 \times 10^5; I_A(0) = 10 \times 10^5; I_S(0) = 2.55525 \times 10^5; R(0) = 10 \times 10^5$ and remaining parameters values are taken from Table 2.

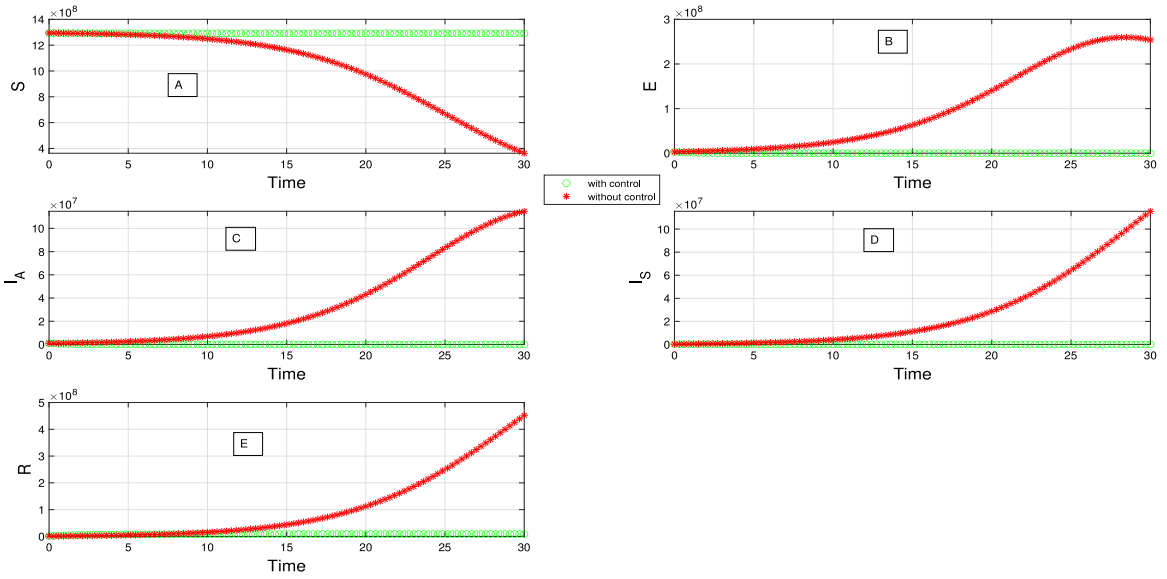

Fig. 12. Optimal Control diagrams for the each compartment.

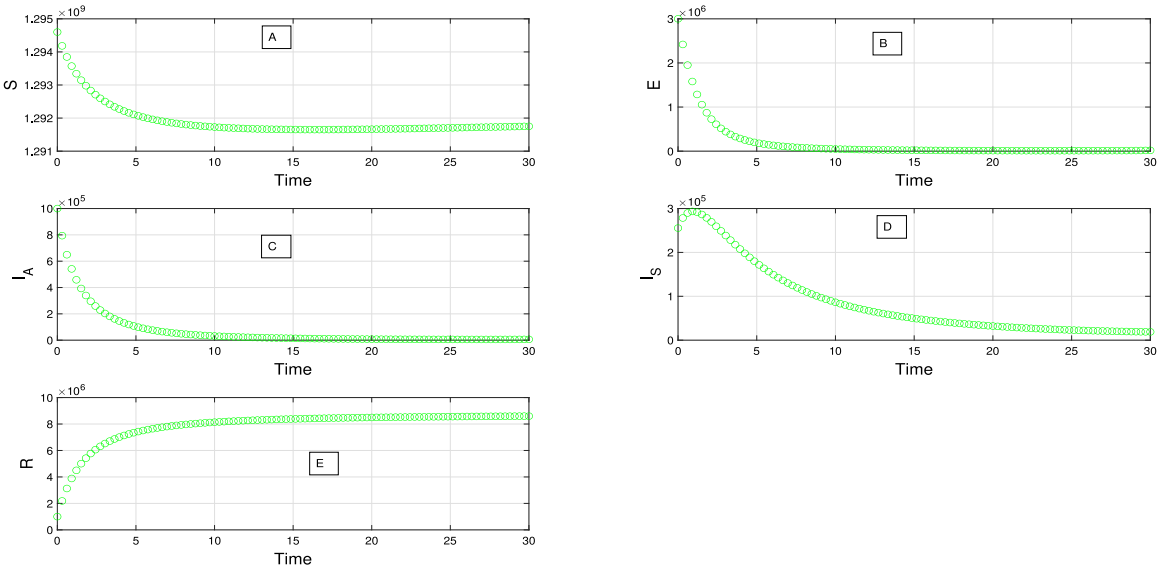

Fig. 13. Control diagrams for the each compartment (Close-up view).

The optimal control graph for the controls $\upsilon_1(t), \upsilon_2(t)$ and $\upsilon_3(t)$ are presented in Figs. 11(A)-11(C). It is obvious from these figures that more effort must be given to the controls, namely, vaccination control $\upsilon_1(t)$ on the exposed class, treatment control on asymptomatic infected class $\upsilon_2(t)$ and treatment control on symptomatic infected class $\upsilon_3(t)$ at the beginning of the disease outbreak. Therefore, it is so important that these controls are applied to the respective compartments at the start of the COVID-19 pandemic in India so that the rapid spread of the disease is controlled.

From Figs. 12(A)-12(E), it is obvious that the populations of the infected compartments are reduced when the optimal control strategies $\upsilon_1(t), \upsilon_2(t), \upsilon_3(t)$ are applied in the compartments E, I_A, I_S respectively. This shows the importance of the implementation of vaccination and treatment controls simultaneously to control the spread of this COVID-19 epidemic in India. From Fig. 13, it is obvious that the populations of the infected compartments, namely, I_A and I_S are reduced drastically when the optimal control strategies $\upsilon_1(t), \upsilon_2(t), \upsilon_3(t)$ are applied simultaneously in the compartments E, I_A, I_S respectively. Further, it is noticed from Fig. 13(E) that the population of the recovered compartment R also increases gradually when the optimal control strategies are applied simultaneously in the respective compartments.

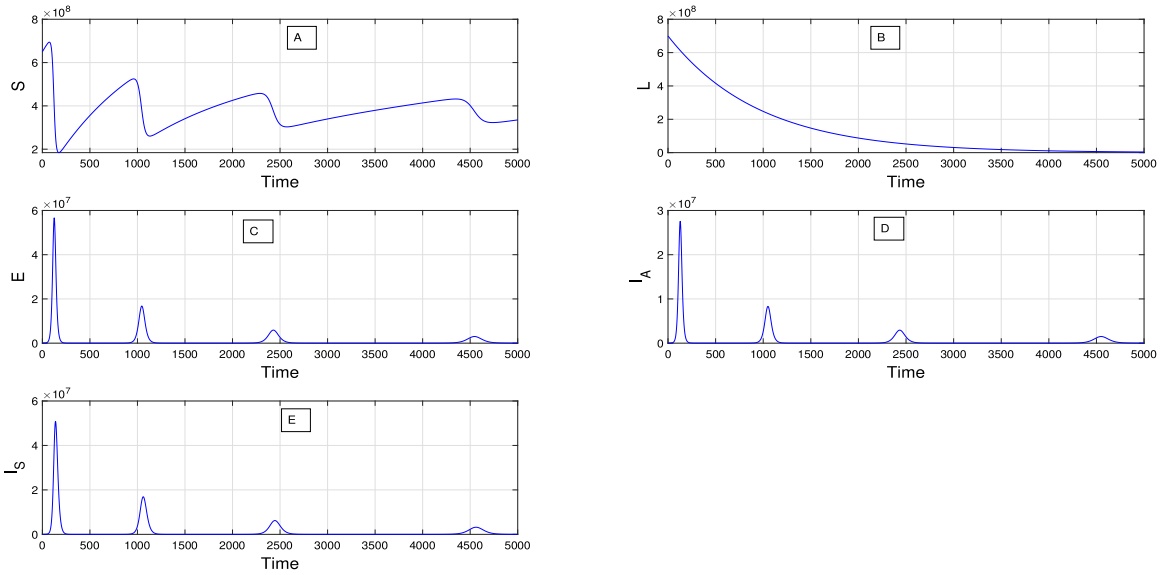

Fig. 14. Time history of the various populations for $\alpha_1 = 0$ with parameters and initial values from Tables 2 and 3 respectively.

From Fig. 14, it is noticed that the single strain COVID-19 waves are formed in our epidemic model when $\alpha_1 = 0$. The study showed that if the lockdown was completely relaxed, a single strain COVID-19 wave was observed.

10. Conclusion

In this paper, we have considered a COVID-19 epidemic model consisting of six population classes, namely, susceptible population (S), lockdown population (L), exposed population (E), asymptomatic infected population (I_A), symptomatic infected population (I_S), recovered population (R) and analyzed the dynamic behavior of the system. The system has two equilibrium points, namely disease-free equilibrium P_0 and endemic equilibrium P_1. The basic reproduction number R_0, which is an important threshold parameter used to study the dynamical behavior of the system, has been calculated and is given by

$$R_0 = \frac{\beta\Lambda(d+\alpha_2)\gamma_1}{d(d+\gamma_1+\gamma_2)(d+\delta_1+\delta_2+\mu_1)(d+\alpha_1+\alpha_2)}$$

It is found that the DFE P_0 is globally asymptotically stable when $R_0 < 1$ and the EE P_1 is globally asymptotically stable under some conditions when $R_0 > 1$. From the sensitivity analysis of R_0 with respect to the parameters α_1, it is noticed that increase in the progression rate from susceptible class to lockdown class makes R_0 decrease and hence the spread of infection in society is drastically reduced. If α_2 increases, i.e., relaxation in lockdown is announced by the Government, then the value of R_0 start increasing steadily and hence there is a rapid spread of the disease in society. Furthermore, the rise of the effective contact rate of infective individuals also increases the value of R_0 which in turn increases the number of infected individuals in the society.

The main aim of this paper is to establish an optimal control problem related to the COVID-19 epidemic model such as to minimize the spread of infection and the cost of treatment. We have used three controls, namely, vaccination control $\upsilon_1(t)$, treatment control $\upsilon_2(t)$ on asymptomatic infected compartment and treatment control $\upsilon_3(t)$ on symptomatic infected compartment.

Theoretical analysis of the dynamics of the COVID-19 model must be supported with numerical analysis, which is achieved by using MATLAB. Figures are created for analyzing the dynamical behavior of the COVID-19 system and comparative figures are presented related to the optimal control problem, which highlights the importance of the controls on the proposed epidemic model. The figures related to the dynamical analysis of the COVID-19 model support the theoretical results. The diagrams related to the optimal control problem indicate that the optimal controls, namely, vaccination and treatment controls are very vital in controlling this epidemic. The graphical analysis of the proposed epidemic model using the values as in Table 2 is presented and the optimal control are obtained theoretically and finally presented graphically. Controlling the spread of the epidemic is a very important task, and it is a vital issue to make detailed studies on control strategies. Predicting and identifying cost-effective control strategies to control the epidemic and minimize the cost of implementing control strategies are important tasks of health administrators and researchers. Many research articles analyzed the dynamics of the COVID-19 models without control strategies with real data belonging to various other countries and the results from our proposed COVID-19 pandemic model considered the data sets from Indian population during the pandemic and it suggested that the COVID-19 epidemic is well controlled by implementing the lockdown, and after analyzing the optimal control problem without lockdown relative to our basic model, we see that control strategies like vaccination and treatment are very effective in controlling the spread of COVID-19 disease in India.

CRediT authorship contribution statement

R. Prem Kumar: Analysis, Wrote the paper. **Sanjoy Basu:** Collected the data, Analysis tools for the paper, Wrote the paper. **P.K. Santra:** Conceived and designed the analysis, Perform the analysis. **D. Ghosh:** Conceived and designed the analysis, Perform the analysis. **G.S. Mahapatra:** Conceived and designed the analysis, Wrote the paper.

Declaration of competing interest

The authors declare that they have no known competing financial interests or personal relationships that could have appeared to influence the work reported in this paper.

Acknowledgments

We are grateful to the Editor and anonymous referees for their valuable comments and helpful suggestions which have helped us to improve the presentation of this work significantly.

Funding

This research work does not have any funding.

References

[1] HealthOrganization W. Coronavirus disease (COVID-19) outbreak. 2019, Available at https://www.who.int/emergencies/diseases/novel-coronavirus-2019 (2020-03-04).
[2] Kumar SU, Kumar DT, Christopher BP, Doss C. The rise and impact of COVID-19 in India. Front Med 2020;7:250.
[3] Jachak S, Phansopkar P, Naqvi MW. Impact of covid-19 in India, a disastrous pandemic outbreak. Int J Res Pharmaceut Sci 2020;11(Special Issue 1).
[4] Pradhan S, Ghose D, Shabbiruddin. Present and future impact of COVID-19 in the renewable energy sector: A case study on India. Energy Sources Part A: Recovery Util Environ Effects 2020;1–11.
[5] Asad A, Srivastava S, Verma MK. Evolution of COVID-19 pandemic in India. Trans Indian Natl Acad Eng 2020;5(4):711–8.
[6] Sarkar K, Khajanchi S, Nieto JJ. Modeling and forecasting the COVID-19 pandemic in India. Chaos Solitons Fractals 2020;139:110049.
[7] Sasikumar K, Nath D, Nath R, Chen W. Impact of extreme hot climate on COVID-19 outbreak in India. GeoHealth 2020;4(12). e2020GH000305.
[8] Bhadra A, Mukherjee A, Sarkar K. Impact of population density on Covid-19 infected and mortality rate in India. Model Earth Syst Environ 2021;7(1):623–9.
[9] Ministry of health and family welfare, Available at https://www.mohfw.gov.in/covid_vaccination/vaccination/index.html.
[10] Yang W, Sun C, Arino J. Global analysis for a general epidemiological model with vaccination and varying population. J Math Anal Appl 2010;372(1):208–23.
[11] Sun C, Hsieh Y-H. Global analysis of an SEIR model with varying population size and vaccination. Appl Math Model 2010;34(10):2685–97.
[12] Zhou X, Cui J. Analysis of stability and bifurcation for an SEIR epidemic model with saturated recovery rate. Commun Nonlinear Sci Numer Simul 2011;16(11):4438–50.
[13] Busenberg S, Cooke K, Thieme H. Demographic change and persistence of HIV/AIDS in a heterogeneous population. SIAM J Appl Math 1991;51(4):1030–52.
[14] Samanta G. Permanence and extinction of a nonautonomous HIV/AIDS epidemic model with distributed time delay. Nonlinear Anal RWA 2011;12(2):1163–77.
[15] Cai L, Guo S, Wang S. Analysis of an extended HIV/AIDS epidemic model with treatment. Appl Math Comput 2014;236:621–7.
[16] Tian JP, Wang J. Global stability for cholera epidemic models. Math Biosci 2011;232(1):31–41.
[17] Bai Z, Zhou Y. Global dynamics of an SEIRS epidemic model with periodic vaccination and seasonal contact rate. Nonlinear Anal RWA 2012;13(3):1060–8.
[18] Lahrouz A, Omari L, Kiouach D, Belmaâti A. Complete global stability for an SIRS epidemic model with generalized non-linear incidence and vaccination. Appl Math Comput 2012;218(11):6519–25.
[19] Wang L, Zhang X, Liu Z. An SEIR epidemic model with relapse and general nonlinear incidence rate with application to media impact. Qual Theory Dyn Syst 2018;17(2):309–29.
[20] Khyar O, Allali K. Global dynamics of a multi-strain SEIR epidemic model with general incidence rates: application to COVID-19 pandemic. Nonlinear Dynam 2020;102(1):489–509.
[21] Betti MI, Heffernan JM. A simple model for fitting mild, severe, and known cases during an epidemic with an application to the current sars-cov-2 pandemic. Infect Dis Model 2021;6:313–23.
[22] Nadim SS, Ghosh I, Chattopadhyay J. Short-term predictions and prevention strategies for COVID-19: a model-based study. Appl Math Comput 2021;404:126251.
[23] Tian H, Liu Y, Li Y, Wu C-H, Chen B, Kraemer MU, et al. An investigation of transmission control measures during the first 50 days of the COVID-19 epidemic in China. Science 2020;368(6491):638–42.
[24] Li M-T, Sun G-Q, Zhang J, Zhao Y, Pei X, Li L, et al. Analysis of COVID-19 transmission in Shanxi province with discrete time imported cases. Math Biosci Eng 2020;17(4):3710.
[25] Sun G-Q, Wang S-F, Li M-T, Li L, Zhang J, Zhang W, et al. Transmission dynamics of COVID-19 in Wuhan, China: effects of lockdown and medical resources. Nonlinear Dynam 2020;101(3):1981–93.
[26] Chen T-M, Rui J, Wang Q-P, Zhao Z-Y, Cui J-A, Yin L. A mathematical model for simulating the phase-based transmissibility of a novel coronavirus. Infect Dis Poverty 2020;9(1):1–8.
[27] Mumbu A-rJ, Hugo AK. Mathematical modelling on COVID-19 transmission impacts with preventive measures: a case study of Tanzania. J Biol Dyn 2020;14(1):748–66.
[28] Rezapour S, Mohammadi H, Samei ME. SEIR epidemic model for COVID-19 transmission by Caputo derivative of fractional order. Adv Difference Equ 2020;2020(1):1–19.
[29] Wijaya KP, Ganegoda N, Jayathunga Y, Götz T, Schäfer M, Heidrich P. An epidemic model integrating direct and fomite transmission as well as household structure applied to COVID-19. J Math Ind 2021;11(1):1–26.
[30] Comunian A, Gaburro R, Giudici M. Inversion of a SIR-based model: A critical analysis about the application to COVID-19 epidemic. Physica D 2020;413:132674.

[31] Engbert R, Rabe MM, Kliegl R, Reich S. Sequential data assimilation of the stochastic SEIR epidemic model for regional COVID-19 dynamics. Bull Math Biol 2021;83(1):1–16.
[32] Rihan FA, Alsakaji HJ, Rajivganthi C. Stochastic SIRC epidemic model with time-delay for COVID-19. Adv Difference Equ 2020;2020(1):1–20.
[33] de Carvalho JaPM, Moreira-Pinto B. A fractional-order model for CoVid-19 dynamics with reinfection and the importance of quarantine. Chaos Solitons Fractals 2021;111275.
[34] Memarbashi R, Mahmoudi SM. A dynamic model for the COVID-19 with direct and indirect transmission pathways. Math Methods Appl Sci 2021;44(7):5873–87.
[35] Farman M, Akgül A, Ahmad A, Baleanu D, Saleem MU. Dynamical transmission of coronavirus model with analysis and simulation. CMES-Comput Model Eng Sci 2021;127(2):753–69.
[36] Koyama S, Horie T, Shinomoto S. Estimating the time-varying reproduction number of COVID-19 with a state-space method. PLoS Comput Biol 2021;17(1):e1008679.
[37] Amar L, Taha A, Mohamed M. Prediction of the final size for COVID-19 epidemic using machine learning: A case study of Egypt. Infect Dis Model 2020;5:622–34. http://dx.doi.org/10.1016/j.idm.2020.08.008.
[38] Biswas SK, Ghosh JK, Sarkar S, Ghosh U. COVID-19 pandemic in India: a mathematical model study. Nonlinear Dynam 2020;102:537–53.
[39] Pizzuti C, Socievole A, Prasse B, Van Mieghem P. Network-based prediction of COVID-19 epidemic spreading in Italy. Appl Netw Sci 2020;5(1):1–22.
[40] Bambusi D, Ponno A. Linear behavior in Covid19 epidemic as an effect of lockdown. J Math Ind 2020;10(1):1–7.
[41] Maheshwari H, Yadav D, Chandra U, Rai D. Forecasting epidemic spread of COVID-19 in India using arima model and effectiveness of lockdown. Adv Math Sci J 2020;9(6):3417–30. http://dx.doi.org/10.37418/amsj.9.6.22.
[42] Sahoo BK, Sapra BK. A data driven epidemic model to analyse the lockdown effect and predict the course of COVID-19 progress in India. Chaos Solitons Fractals 2020;139:110034.
[43] de Sousa LE, de Oliveira Neto PH, da Silva Filho DA. Kinetic Monte Carlo model for the COVID-19 epidemic: Impact of mobility restriction on a COVID-19 outbreak. Phys Rev E 2020;102(3):032133.
[44] De la Sen M, Ibeas A, Agarwal R. On confinement and quarantine concerns on an SEIAR epidemic model with simulated parameterizations for the covid-19 pandemic. Symmetry 2020;12(10):1–36. http://dx.doi.org/10.3390/sym12101646.
[45] Yuan R, Ma Y, Shen C, Zhao J, Luo X, Liu M. Global dynamics of COVID-19 epidemic model with recessive infection and isolation. Math Biosci Eng MBE 2021;18(2):1833–44.
[46] Hikal M, Elsheikh M, Zahra W. Stability analysis of COVID-19 model with fractional-order derivative and a delay in implementing the quarantine strategy. J Appl Math Comput 2021;1–27.
[47] Mishra BK, Keshri AK, Rao YS, Mishra BK, Mahato B, Ayesha S, et al. COVID-19 created chaos across the globe: Three novel quarantine epidemic models. Chaos Solitons Fractals 2020;138:109928.
[48] Jiao S, Huang M. An SIHR epidemic model of the covid-19 with general population-size dependent contact rate. AIMS Math 2020;5(6):6714–25. http://dx.doi.org/10.3934/math.2020431.
[49] Hu J, Hu G, Cai J, Xu L, Wang Q. Hospital bed allocation strategy based on queuing theory during the covid-19 epidemic. Comput Mater Contin 2021;66(1):793–803. http://dx.doi.org/10.32604/cmc.2020.011110.
[50] Amaku M, Covas DT, Coutinho FAB, Neto RSA, Struchiner C, Wilder-Smith A, et al. Modelling the test, trace and quarantine strategy to control the COVID-19 epidemic in the state of São Paulo, Brazil. Infect Dis Model 2021;6:46–55.
[51] Abbasi Z, Zamani I, Mehra AHA, Shafieirad M, Ibeas A. Optimal control design of impulsive SQEIAR epidemic models with application to COVID-19. Chaos Solitons Fractals 2020;139:110054.
[52] Bonnans JF, Gianatti J. Optimal control techniques based on infection age for the study of the COVID-19 epidemic. Math Model Nat Phenom 2020;15:48.
[53] Castilho C, Gondim J, Marchesin M, Sabeti M. Assessing the efficiency of different control strategies for the covid-19 epidemic. Electron J Differential Equations 2020;2020:1–17.
[54] Elie R, Hubert E, Turinici G. Contact rate epidemic control of COVID-19: an equilibrium view. Math Model Nat Phenom 2020;15:35.
[55] Kantner M, Koprucki T. Beyond just "flattening the curve": Optimal control of epidemics with purely non-pharmaceutical interventions. J Math Ind 2020;10(1):1–23.
[56] Lobato FS, Libotte GB, Platt GM. Identification of an epidemiological model to simulate the COVID-19 epidemic using robust multiobjective optimization and stochastic fractal search. Comput Math Methods Med 2020;2020.
[57] Parag KV, Donnelly CA. Using information theory to optimise epidemic models for real-time prediction and estimation. PLoS Comput Biol 2020;16(7):e1007990.
[58] Kouidere A, Youssoufi LE, Ferjouchia H, Balatif O, Rachik M. Optimal control of mathematical modeling of the spread of the COVID-19 pandemic with highlighting the negative impact of quarantine on diabetics people with cost-effectiveness. Chaos Solitons Fractals 2021;145:110777.
[59] Baba IA, Nasidi BA, Baleanu D. Optimal control model for the transmission of novel COVID-19. Comput Mater Contin 2021;66(3):3089–106.
[60] Choi W, Shim E. Optimal strategies for social distancing and testing to control COVID-19. J Theoret Biol 2021;512:110568.
[61] Hu L, Nie L-F. Dynamic modeling and analysis of COVID-19 in different transmission process and control strategies. Math Methods Appl Sci 2021;44(2):1409–22.
[62] Benahmadi L, Lhous M, Tridane A. Mathematical modeling of COVID-19 in Morocco and the impact of controlling measures. Commun Math Biol Neurosci 2021;2021:Article–ID.
[63] Li Q, Tang B, Bragazzi NL, Xiao Y, Wu J. Modeling the impact of mass influenza vaccination and public health interventions on COVID-19 epidemics with limited detection capability. Math Biosci 2020;325:108378.
[64] Gonçalves A, Maisonnasse P, Donati F, Albert M, Behillil S, Contreras V, et al. SARS-CoV-2 viral dynamics in non-human primates. PLoS Comput Biol 2021;17(3):e1008785.
[65] Birkhoff G, Rota GC. Ordinary differential equations. 4th ed.. Wiley; 1989.
[66] Khanh NH. Stability analysis of an influenza virus model with disease resistance. J Egypt Math Soc 2016;24(2):193–9.
[67] Van den Driessche P, Watmough J. Reproduction numbers and sub-threshold endemic equilibria for compartmental models of disease transmission. Math Biosci 2002;180(1–2):29–48.
[68] Mishra BK, Keshri AK, Saini DK, Ayesha S, Mishra BK, Rao YS. Mathematical model, forecast and analysis on the spread of COVID-19. Chaos Solitons Fractals 2021;147:110995.
[69] Kot M. Elements of mathematical ecology. Cambridge University Press; 2001.
[70] Hirsch WM, Hanisch H, Gabriel J-P. Differential equation models of some parasitic infections: methods for the study of asymptotic behavior. Comm Pure Appl Math 1985;38(6):733–53.
[71] Khatua A, Kar TK. Dynamical behavior and control strategy of a dengue epidemic model. Eur Phys J Plus 2020;135(8):1–22.
[72] Blayneh K, Cao Y, Kwo H-D. Optimal control of vector-borne disease: Treatment and prevention. Discrete Contin Dyn Syst Ser B 2009;11(3):587–611.
[73] Joshi HR. Optimal control of an HIV immunology model. Optim Control Appl Methods 2002;23(4):199–213.
[74] Gabriela M, Gomes M, White LJ, Medley G. Infection, reinfection, and vaccination under episuboptimal immune protection: epidemiological perspectives. J Theoret Biol 2004;228(4):539–49.
[75] Sharma S, Samanta G. Analysis of a hand–foot–mouth disease model. Int J Biomath 2017;10(02):1750016.
[76] Zaman G, Kang YH, Cho G, Jung IH. Optimal strategy of vaccination & treatment in an SIR epidemic model. Math Comput Simulation 2017;136:63–77.
[77] Lukes D. Differential equations: classical to controlled, in : mathematics in science and engineering, Vol. 162. New York: Academic Press; 1982.
[78] Kamien M, Schwartz N. Dynamics optimization: the calculus of variations and optimal control in economics and management. The Netherland: Elsevier Science; 2000.